Composites Part B 242 (2022) 110048

Contents lists available at ScienceDirect

Composites Part B

journal homepage: www.elsevier.com/locate/compositesb

Effect of silica aerogel on thermal insulation and acoustic absorption of geopolymer foam composites: The role of aerogel particle size

Y.X. Chen [a,b,1], K.M. Klima [b,1], H.J.H. Brouwers [b], Qingliang Yu [a,b,*]

[a] School of Civil Engineering, Wuhan University, Wuhan, 430072, PR China
[b] Department of the Built Environment, Eindhoven University of Technology, P.O. Box 513, 5600 MB, Eindhoven, the Netherlands

ARTICLE INFO

Keywords:
Silica aerogel
Geopolymer
Hygrothermal performance
Thermal insulation
Acoustic absorption
Foam render

ABSTRACT

Silica aerogel features super thermal insulating and excellent sound absorption. Although the application of silica aerogel in building materials for energy saving has been investigated recently, the role of aerogel particle size on geopolymer foam render can be crucial but is rarely studied. In this research, four kinds of silica aerogel with different particle sizes (2–40 μm, 100–700 μm, 100–1200 μm, 700–4000 μm) are applied in geopolymer foam aerogel render (GFAR) to improve the thermal insulation and acoustic absorption performance. Results show that larger silica aerogel particles are more beneficial for acoustic absorption and thermal insulation while smaller aerogel particles are less effective for insulation properties. The microstructure of GFAR is investigated in-depth with micro-CT, optical microscopy and ultrasonic pulse velocity test. The mechanism of the improved performance of GFAR with different silica aerogel is explained. The optimal geopolymer foam aerogel render (GFAR) reaches a thermal conductivity of 0.133 W/(m·K), an average value of acoustic absorption coefficient of 0.51 with a density of 715.2 kg/m^3. The result of this study is essential to enlighten the use of larger silica aerogel particles in geopolymer foam render, focusing on a low dosage of silica aerogel while utilize its full benefit.

1. Introduction

The energy-saving of the building sector and the comfort of the indoor living environment have received rising attention due to the increasing awareness of sustainability and the quality of life [1]. The building industry is responsible for almost 40% of the total energy and CO_2 emission in developed countries [2]. For now, many countries have already initiated policies to decrease heat loss through building shells [3]. Moreover, the functionalization of insulation materials is also very important, for instance, improving the acoustic absorption performance to increase the quietness of the indoor environment [4,5] and reduce the noise pollution generated from daily life [6]. Therefore, developing newly high-performance insulating lightweight materials is of significant urgency.

Silica aerogel is a super-insulating inorganic material [7], consisting of a 3D network of crosslinking silica nanoparticles and 95%–99% of air [8]. Thanks to the high porosity and low solid thermal conductivity (λ), the effective thermal conductivity of silica aerogel is pretty low, normally achieving 0.012–0.018 W/(m·K) [9]. However, the silica aerogel is very brittle and easy to break, the commercial silica aerogels are always produced in a powder or particle form [10]. It is often incorporated in other matrices, like fibreglass mats or other lightweight materials to facilitate its benefits [11]. Several investigations related to the incorporation of silica aerogel in building materials have already been carried out as presented in Table 1. Ng et al. [12] prepared high-performance aerogel concrete, with bulk density and thermal conductivity of 1300 kg/m^3 and 0.4–0.5 W/(m·K), respectively. The concrete has a low water to binder ratio of 0.20–0.25 and a silica aerogel replacement ratio of 50%–70% with sand. Tao et al. [13] developed normal cement mortar with an aerogel replacement ratio of 60%, featuring a compressive strength of 8.3 MPa and thermal conductivity of 0.26 W/(m·K). Júlio et al. [14] prepared lightweight aerogel aggregate concrete with a 100% replacement ratio of silica aerogel with sand, resulting in concrete with very low thermal conductivity of 0.085 W/(m·K) but compressive strength of only 0.41 MPa. Seo et al. [15] investigated the silica aerogel used in fly ash/slag geopolymer concrete, with an aerogel concentration of 25%–75%. However, the thermal conductivity is relatively high, reaching 0.8 W/(m·K). Zhu et al. [16] investigated the cement-based mortars and coatings with the addition of silica aerogel. The thermal conductivity is low (0.17 W/(m·K)) with a

* Corresponding author. School of Civil Engineering, Wuhan University, Wuhan, 430072, PR China.
E-mail address: q.yu@bwk.tue.nl (Q. Yu).
[1] Authors contribute equally to this work.

https://doi.org/10.1016/j.compositesb.2022.110048
Received 11 December 2021; Received in revised form 2 June 2022; Accepted 6 June 2022
Available online 18 June 2022

compressive strength of 1.4 MPa.

Above all, the silica aerogels are mainly used as a replacement for normal-weight aggregate to reduce thermal conductivity and improve insulating properties. However, only a few researchers have investigated the effect of particle size of silica aerogel on the insulation property and the sound absorption of the prepared lightweight materials. For instance, Buratti et al. [17] studied the influence of particle size of silica aerogel on the thermal and acoustic properties of aerogel particles. Their results show the smallest particle size has a better performance than larger silica aerogel in terms of insulation properties. Moreover, they developed innovative aerogel based plasters and studied their thermal and acoustic performance [18]. Spagnol et al. [19] investigated the influence of the type of packing and number of spherical aerogel on the modelling of thermal conduction. These studies provide insights into the effect of silica aerogel size on the performance of lightweight building materials. However, the concentration of silica aerogel is relatively high, indicating the high cost of the resulting materials, which is hard to apply in the real world. Therefore, finding a smart method to use silica aerogel and choosing a cost-effective lightweight building material for silica aerogel to facilitate its ultra-insulating performance is very important.

In order to solve the problems, an optimization can be made - either by reducing the amount of silica aerogel used or by using ultra-lightweight matrix. In addition, replacing Portland cement-based matrix by geopolymer which possesses superior thermal properties, can be applied to optimize composite mixture and maintain a sufficient thermal and acoustic performance.

Thermal insulating renders are the potential materials in this regard, with the thermal conductivities normally lower than 0.2 W/(m·K) and density falling in ultralightweight concrete [21]. Foam render is a kind of insulating material, however, with high energy consumption due to the use of cement, which is responsible for 7% of CO_2 emissions around the world [22]. From the point of reducing the CO_2 footprint and cost, geopolymer foam render is a promising choice. Fly ash-based geopolymer is a promising alternative building material, which is obtained via activation of aluminosilicate source, e.g. fly ash, by highly alkaline silicate solution (MOH and M_2SiO_3 M = Na, K) [23]. Moreover, the use of industrial by-products in geopolymer features low energy consumption and is environmentally friendly, providing enhanced sustainability from material manufacture to construction operation [24]. Apart from the environmental aspect, geopolymer is a promising binder for thermal insulators due to its relatively low thermal conductivity [25]. However, for some applications a significant thermal conductivity coefficient reduction is needed. As a result, exploring a further method of decreasing its thermal conductivity is a current area of interest. Thus, to attain the required effects, the material must be enriched with a phase of a much lower thermal conductivity, such as silica aerogel. Huang et al. [26] demonstrated that combining geopolymer with silica aerogel may provide low thermal conductivity and sufficient mechanical properties, demonstrating the possibility of manufacturing an aerogel/geopolymer composite for insulation applications.

Another route for obtaining a material with a lower thermal conductivity is to introduce air as the low thermal conductivity phase, resulting in a foam composite [27]. In order to create the porous structure of geopolymer foam concrete, methods including chemical foaming agents or mechanical foaming techniques can be used, all providing large numbers of pores inside the geopolymer matrix [27].

. Certain techniques, nevertheless, may be more appropriate depending on the intended pore structure. When using chemical aeration, hydrogen peroxide (H_2O_2) is the cheapest and easiest to operate [28]. Surfactant specificities and mixing ability, on the other hand, can be used to lower their total critical micelles concentration (CMC), resulting in a large number of micelles produced and better foam stability. A rise in the quantity of H_2O_2 alone may lead to the escape and aggregation of air bubbles, and therefore promote the creation of large air voids, further reducing mechanical strength [29] and affecting sound absorption ability. When the concentration of the foaming agent is increased, the number of bubbles decreases while their diameter increases [30]. Although increasing the amount of surfactants can help to mitigate the detrimental effects of this phenomenon, research shows that excessive concentration of surfactants has a negative impact on compressive strength [31]. Reducing surfactant concentrations, in turn, will diminish the total volume of connected pores, which has a negative effect on acoustic absorption. Moreover, this will result in a narrower pore size distribution with a larger proportion of voids that is less preferable [32].

In addtion, another concern about the use of highly porous concrete is its high water uptake [33]. The wetting and drying of the porous building materials could result in different thermal transfer behaviour through the building envelop [34]. It is acknowledged that hydrophobic particles [35], such as silica aerogel could increase the hygrothermal properties in insulation renderings [36], however, the effect of granular size of silica aerogel has not been studied yet. Also, the acoustic absorption of plain foam concrete is relatively low, due to the low pore interconnectivity with lack of multiscale pore sizes in the matrix. Therefore, a further increase in thermal insulation and acoustic absorption, meanwhile a reduction in moisture transport through the foam concrete is desired.

The application of silica aerogel is hypothesized to not only increase the porosity of the material but also maintain a wide range of pore sizes and minimize bubble coalescence. Further, owing to the surface modification of silica hydrogel during preparation with the silanes [37], the hydrophobic characteristics of the aerogel may counterbalance the detrimental effect of air humidity that can influence the thermal insulation of GFAR [38]. However, commercial silica aerogel has different forms and sizes. Normally, due to the difficulty in preparing monolithic silica aerogel, most of the silica aerogel is in the form of particles. The particle size can significantly differ depending on the processing parameters, ranging from 2 μm to 4000 μm. Silica aerogel with different particle sizes could function quite differently on the insulation performance of foam render. For instance, Halim et al. [39] looked into the

Table 1
Comparison of lightweight insulating concrete with the addition of silica aerogel.

Authors	Raw materials	w/b	AG RR/PS	BD (g/cm^3)	CS (MPa)	TC (W/(m·K))	Literature
Ng et al.	CEM, quartz fines, SF, AG, SP	0.2–0.25	0–80% 0.01–4 mm	0.8–2.3	5–150	0.3–2.3	[12]
Ng et al.	CEM, quartz fines, SF, sand, AG, SP	0.2	60–70% 0.01–4 mm	~	5–19	0.12–0.53	[20]
Tao et al.	CEM, SF, sand, SP and AG.	0.4	0–60% 2~4 mm	1.00–1.98	8.3–60	0.26–1.86	[13]
Júlio et al.	CEM, AG, surfactant	0.66–1.2	100%	0.218–0.412	~	0.080–0.098	[14]
Seo et al.	FA, slag, activator, AG	0.5	25/50/75%	1.28–1.53	13–28	0.9–1.8	[15]
Zhu et al.	CEM, SF, SP, Sand, AG	0.4	33–67% 1.2–4 mm	0.74–1.55	1.4–13.0	0.17–0.40	[16]

Note: AG-aerogel, CEM-cement, SF-silica fume, SP-superplasticizer, RR-replacement ratio, PS-particle size, BD-bulk density, CS-compressive strength, TC-thermal conductivity, w/b-water to binder ratio.

effect of silica aerogel particle size on thermal insulation and observed that bigger particles provide better insulation for produced matrix made of unsaturated polyester resin. However, the mechanism of particle size of aerogel on different properties of insulating cementitious materials remains unclear. Kucharek et al. [40] revealed that small aerogel particles had a minor impact on the thermal and mechanical characteristics of epoxy resin. The composite system evaluated in this research revealed that adding more small aerogel particles over a specific concentration does not affect the heat conductivity and compression characteristics. However, further study was recommended to fully comprehend this phenomenon.

In this study, a geopolymer foam aerogel render (GFAR) with the addition of a low dosage silica aerogel is prepared, with the special focus on the effects of particle sizes of aerogel on the thermal insulating at different humidities and acoustic absorption performance. Four different kinds of silica aerogel are selected for this purpose. The microstructure of geopolymer foam aerogel render (GFAR) is investigated through optical microscopy, micro-CT, and UPV test. The performances of GFAR are measured by thermal conductivity test and acoustic impedance tube method. The results of this research shed light on the smart application of silica aerogel in ultralightweight foam concrete.

2. Materials and methodology

2.1. Starting materials

Four different kinds of silica aerogel were purchased from Cabot, which are IC3100, IC3110, IC3120 and LA1000. The difference between the silica aerogels are the particle size and the translucency of the aerogel. The particle size of IC3100, IC3110, IC3120 and LA1000 are 2–40 μm, 100–700 μm, 100–1200 μm and 700–4000 μm, respectively. The particle size distribution of silica aerogel is shown in Fig. 1 (a), measured with laser light scattering, except for LA1000 due to the limitation of the device (Mastersizer 2000). The particle size of LA1000 is calculated from sieving. The physical properties of aerogel are shown in Table 2. The TEM image is shown in Fig. 1 (b), showing a nanoporous structure and a

Table 2
Physical properties of the four types of silica aerogel.

Groups	Particle size[a] (μm)	SSA (m^2/g)	Pore size (nm)	BD (g/cm^3)[a]	TC[a] (W/(m·K))
IC3100	2–40	699	14.0	0.12–0.15	0.012
IC3110	100–700	688	12.5	0.12–0.15	0.012
IC3120	100–1200	694	13.1	0.12–0.15	0.012
LA1000	700–4000	683	12.4	0.12–0.15	0.018

[a] Data provided by Cabot. SSA-Specific surface area; BD: Bulk density; TC-Thermal conductivity.

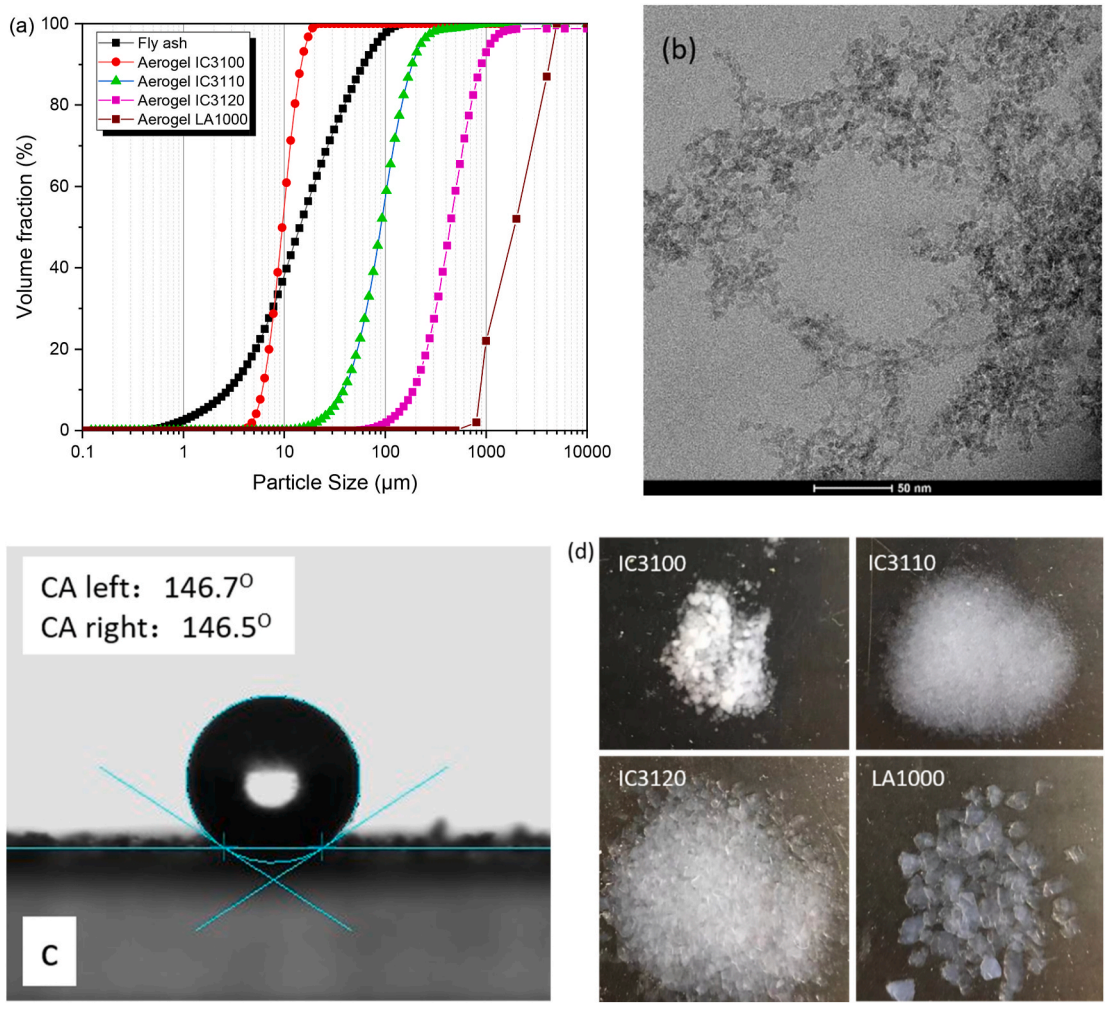

Fig. 1. (a) Particle size distribution of fly ash and silica aerogel (b) TEM of silica aerogel (c) water contact angle of IC3100 (d) morphology of four types of silica aerogel.

3D network of silica nanoparticles. Fig. 1 (c) shows the water contact angle of IC3100, reaching 146.6°. Therefore, the silica aerogel is highly hydrophobic. Fig. 1 (d) shows the morphology of the four types of silica aerogel used. The main difference is the particle size of silica aerogel and its transparency.

For the preparation of geopolymer matrix, the silica modulus of SiO_2/K_2O 1.4 and 5.5% K_2O was achieved by combining potassium hydroxide pellets (VWR life science, reagent grade) and potassium-silicate solutions (WHC GmbH, K_2O 8%, SiO_2 20.8%, 72.8% H_2O by mass). As-prepared activator solution was stored for a period of 24 h to reach equilibrium before application for geopolymer preparation. Hydrogen peroxide (30% Sigma-Aldrich, Germany) was utilized as a chemical foaming agent in combination with the surfactant mix solution, non-ionic Triton X-100 (VWR chemicals) and anionic sodium dodecyl sulfates (SDS) (98% purity, Sigma-Aldrich, Germany). Coal combustion fly ash class F (Vliegasunie B.V.) was utilized as the solid precursor for geopolymer production in this investigation. Tables 3 and 4 show the oxide and mineral compositions, which were used to calculate the potential reactivity of fly ash (Table 5) [41].

2.2. Preparation of the geopolymer foam aerogel concrete

The mix design of the paste is shown in Table 6. The detailed preparation process is as follows:

(1) Dry components homogenization

The dry components (fly ash and silica aerogel) were mixed in a 5-L Hobart mixer until homogenized (60s) at a low mixing speed to avoid silica aerogel breakage. The experimental conditions were: indoor temperature of 23 °C and relative humidity of 50%.

(2) Slurry preparation

Homogenized powder and the activator solution were stirred and mixed evenly at low speed (30 s). The mixing was stopped to guarantee that there are no powdery remains on the bottom and sides of the mixer, and rested for 60 s to allow sufficient contact between materials. Furthermore, the slurry was mixed at high speed for 60 s.

(3) Foaming

A foaming ingredient, hydrogen peroxide (30%), was introduced while mixing at low speed, followed by two prepared surfactants, Sodium Dodecyl Sulphate and Triton X-100. After adding the surfactants, the rotation speed was raised, and the paste was stirred for 30 s under the same, controlled indoor conditions: 23 °C and relative humidity of 50%.

(4) Casting and hardening

The pastes were cast into the moulds of 40 × 40 × 160 mm^3, 100 × 100 × 100 mm^3 and cylindrical moulds H:50 mm r:40 mm. All samples were sealed with a plastic film and cured for 24 h at 23 °C, RH 50%.

(5) Demoulding and curing

After 24 h the samples were demolded, wrapped in a plastic film and cured for 24 h at 60 °C in the oven.

(6) Aging

After the elevated temperature curing, specimens were stored for a further 26 days at room temperature (23 °C) and relative humidity of 50% ± 5%

2.3. Characterization

2.3.1. Density and porosity of GFAR

The oven dry density of the prepared GFCA was measured by the simple mass to volume ratio, according to EN 12350-1 [42]. The prepared samples were first dried at 105 °C in an oven until a constant mass. The skeleton density of the prepared samples was measured by a density analyser Helium pycnometer (AccuPyc II 1340 Micromeritics), according to EN 1097-7 [43]. The results are acquired based on the mean value of three testing specimens. The porosity of the GFCA was calculated according to:

$$\Phi = \left(1 - \frac{\rho_b}{\rho_s}\right) \times 100\% \quad (1)$$

where ρ_b is the dry bulk density of the GFAR, ρ_s is the skeleton density of the GFAR, Φ is the porosity of the GFAR.

2.3.2. Thermal conductivity and acoustic absorption

The thermal conductivity of the GFAR was measured with a heat transfer analyser (ISOMET model 2104), according to the standard ASTM D 5930. The analyzer applies a dynamic measurement method to determine simultaneously the volumetric heat capacity (J/(m^3·K)) and the thermal conductivity (W/(m·K)) of materials with a measurement time of about 8–16 min. The measurement is based on the analysis of the temperature response of the tested sample to heat flow impulses, while the heat flow is excited by electrical heating of a resistor heater inserted into the probe which is in direct contact with the test sample. Three probes with different thermal conductivity measurement ranges of 0.04–0.3, 0.3–2.0 and 2.0–6.0 W/(m·K) with an accuracy of 5% of reading plus 0.001 W/(m·K) are equipped. The ambient temperature during the testing was constant at around 20 °C. The average thermal conductivity of three test specimens was calculated as the final thermal conductivity of the GFAR. The testing image of the thermal conductivity of GFAR is shown in Fig. 2.

The acoustic absorption test for GFAR was conducted with an impedance tube method as shown in Fig. 3. The hardened cylinder GFAR samples with a dimension of a height of 50 mm/20 mm and a diameter of 40 mm were tested. According to Li et al. [44], the minimum thickness of a porous material should normally be no less than 1/4 wavelength in order to absorb all incident sound (2000 Hz, 0.172 m). In specific, the measurement principle is through generating a plane wave by a loudspeaker on the one side of the tube that was then spreading through the tube before reflecting by the GFAR. The GFAR changes the reflected wave and by collecting the generated standing wave, the sound absorption coefficient of the samples can be determined. The wave was measured at six different locations in the tube. This was done to increase the accuracy as described in the measurement protocol for the impedance tube. GFAR samples were inserted at the end of the impedance tube and backed by a rigid surface.

Table 3
Chemical composition of fly ash and silica aerogel.

Composition (%)	CaO	SiO_2	Al_2O_3	Fe_2O_3	K_2O	Na_2O	SO_3	MgO	TiO_2	MnO	SSA (m^2/g)	SD (g/cm^3)
Fly ash	6.1	54.5	21.5	9.1	2.8	0.4	1.3	1.3	0.9	2.0	0.4 ± 0.1	2.2 ± 0.2
Silica aerogel	–	99.6	–	–	–	–	–	–	–	–	680 ± 25	0.10 ± 0.01

Note: SSA: Specific surface area; SD: Specific density.

Table 4
Phase quantification via Rietveld refinement of fly ash.

Amorphous (%)	Quartz (%)	Mullite (%)	Hematite (%)	Periclase (%)	Magnetite (%)	Anatase (%)
ICSD	83849	66451	22505	9863	85807	24276
84.99 (0.30)	5.03 (0.09)	7.19 (0.16)	1.69 (0.12)	0.56 (0.09)	0.24 (0.09)	0.22 (0.05)

Note: Uncertainty in the brackets, as taken from Topas.

Table 5
Potential reactivity of fly ash.

	Moles of Si per 100 g of FA	Moles of Al per 100 g of FA	Si/Al molar ratio
Total content (XRF)	0.9071	0.7969	1.14
Crystalline content (XRD)	0.1170	0.1018	1.15
Amorphous content	0.7901	0.6951	1.14

Also, the average values of the coefficient of absorption were calculated for each sample, which is defined as the area under the absorption curves normalized over the frequency range and determined as shown in the equation below, where f_1 is the lower frequency at 100 Hz and f_2 is the upper frequency at 2500 Hz, according to ASTM C384-4 [17]:

$$\alpha_{med} = [1/f_2 - f_1]\int_{f_1}^{f_2} \alpha(f)df \quad (2)$$

where α_{med} is the average values of the coefficient of absorption, f is the frequency at a certain range.

2.3.3. Compressive and flexural strength

The GFAR samples with the size of 40 × 40 × 160 mm^3 were used to determine the flexural strength at 7 and 28 days, following EN196-1 [45]. The GFAR samples with the size of 40 × 40 × 40 mm^3 were used to determine the compressive strength at 7 and 28 days, following EN196-1 [45]. The average strength of three test specimens was calculated as the final strength of the GFAR.

2.3.4. Micro-CT

For pore size and silica aerogel particle dispersion analysis, μCT 100, Scanco Medical AG, Switzerland scanner was used. The scanning voltage was applied to 70 kV, and the X-ray current was set at 200 mA. A 0.5 mm aluminium filter was used to lower the beam's hardness. 205 images with a 2048 × 2048 resolution were generated in a single measurement, each sample was measured three times at different specimen heights, with a voxel size of 10 μm. In preparing binarization processes and separating air voids and aerogel silica particles from the denser geopolymeric matrix, 3D-reconstruction program was utilized. As a result, in the examination of pore size distribution and open porosity, the two media were regarded as a single-air-derived medium.

2.3.5. UPV test

Ultrasonic pulse velocity (UPV) test was used to measure the compactness and voids of GFAR samples, following ASTM C597-02 [46]. Pulses of longitudinal stress waves are generated by an electro-acoustical transducer that is held in contact with one surface of the concrete under test. After traversing through the concrete, the pulses are received and converted into electrical energy by a second transducer located a distance L from the transmitting transducer. The transit time T is measured electronically. The pulse velocity V is calculated by dividing L by T. Direct method was used during the whole test, which requires access to two surfaces of the concrete cubes. A viscous grease is used to ensure efficient transfer of energy between the concrete and the transducers. Each specimen was tested twice, and the average value was determined as the final velocity of the foam concrete.

2.3.6. Water uptake and water contact angle

The applied test method was according to the standard method described in ISO 12571:2013E [47]. A measurement was performed in a climate chamber capable of maintaining relative humidity within 5% and temperature within 2 °C. The specimens were dried in a drying oven at 105 °C until they reached a constant mass (mass change less than 0.1% of the total mass). The specimens in the climate chamber were initially conditioned at the lowest specified humidity level from the test range (30%, 60%, 80%) at a constant temperature of 23 °C. The samples were weighed regularly until they reached equilibrium with the environment. The water uptake (WU) was determined as the difference between the mass of the dry sample and conditioned in a climate chamber specimen, and the thermal conductivity was determined using the

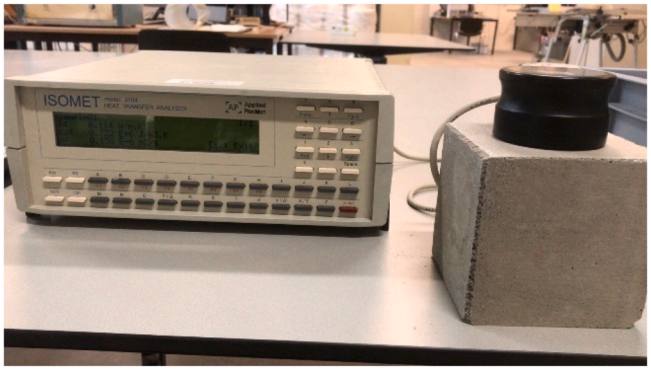

Fig. 2. Measurement of thermal conductivity of GFAR.

Table 6
Recipe of geopolymer foam aerogel render (GFAR) (kg/m^3).

Groups	FA	Activator	HP	SDS	TX100	IC3100	IC3110	IC3120	LA1000
Ref	1172	421.9	7.9	3.5	2.6	–	–	–	–
AG1-10	1055	379.7	7.1	3.1	2.3	8.87	–	–	–
AG2-10	1055	379.7	7.1	3.1	2.3	–	8.87	–	–
AG3-10	1055	379.7	7.1	3.1	2.3	–	–	8.87	–
AG4-10	1055	379.7	7.1	3.1	2.3	–	–	–	8.87
AG5-10	1055	379.7	7.1	3.1	2.3	0.67	1.67	2.87	3.67
AG6-20	938	337.5	6.3	2.8	2.1	1.33	3.34	5.74	7.34

Note: HP-Hydrogen peroxide; SDS-Sodium dodecyl sulphate; TX100-Triton X 100; FA-Fly Ash; Aerogel volume percentage was 10%, except for AG6-20 group, where 20 vol% aerogel was added.

Fig. 3. Measurement of acoustic absorption of GFAR.

technique described above. Cubic samples with dimensions of 100 × 100 × 100 mm^3 were used in this investigation.

$$WU = \frac{(m_1 - m_0)}{m_0} \times 100\% \quad (3)$$

where WU is the water uptake, m_0 is the initial mass of the sample, m_1 is the final mass of the sample after being stored at 80% humidity environmental chamber.

The hydrophobicity of silica aerogel was measured with a Dataphysics Contact Angle System. The silica aerogel powder was evenly distributed on a slide with a double-sided tape after being milled to pass an 80 μm sieve. The volume of the Milli-Q water droplet used for contact angle testing was 3 μL.

2.3.7. Microstructure observation

2.3.7.1. Optical microscopy. A ZEISS Axio Imager equipped with ZEISS Axiocam 305 CAMERA Colour, Z2 optical microscope (Carl Zeiss, Göttingen, Germany) was used to examine the microstructure morphology and silica aerogel particle location in the geopolymeric matrix. An objective lens Zeiss EC Epiplan Neofluar 5x BD was used for each measurement.

2.3.7.2. TEM. The microstructure of silica aerogel was observed with transmission electron microscopy (TEM), conducted with a Tecnai 20 operated at 200 kV. The sample was prepared by breaking it into smaller pieces with the use of liquid nitrogen and then applying it on a Cu 200 mesh grid with a carbon support layer.

3. Results and discussions

3.1. Physical and mechanical properties of GFAR

The obtained materials (Fig. 4) were subjected to the characteristics of the bulk density, skeleton density, porosity, and compressive strength of the GFAR, as presented in Fig. 6. It can be observed that the dry bulk density is related to the particle size and the dosage of aerogel. The more silica aerogel in the GFAR fresh paste, the lighter the paste could be. This is due to the silica aerogel particles occupying some of the solid parts in the fresh paste. It is noteworthy that the lowest density is achieved for the AG6-20 sample, in which the aerogel content reaches 20% of the total volume of the paste. Therefore, it can be stated that the addition of silica aerogel could result in the formation of more voids that are provided by the aerogels.

Further, the particle size of silica aerogel has a significant influence on the bulk density of GFAR. It can be observed that AG1-10 has the highest density while AG4-10 has the lowest bulk density among samples with 10% replacement. The reason could be attributed to the fineness of the silica aerogel. Fig. 5 shows the difference between the optimal mix curve and the actual curve of the mix from AG1-10 to AG5-10. The optimal packing is calculated according to the modified A&A model, as reported in a previous study [5]. It can be observed the optimal packing curve is close to the actual curve of the AG1-10 sample, which means enhanced packing. While with the increasing particle size of the silica aerogel, the deficit between the optimal packing curve and the actual packing curve increases significantly. It indicates the inter-particle porosity will increase with the increasing particle size of silica aerogel. Consequently, the bulk density of GFAR will decrease.

The AG1-10 sample contains 10 vol % 2–40 μm silica aerogel, so the addition of silica aerogel could result in better packing of the materials, leading to a denser matrix. However, with the increasing particle size of the aerogels, the deviation between optimal packing and real packing curves becomes larger. Hence, with the incorporation of much larger silica aerogel granules, the inter-particle porosity will be higher, thus obtaining a looser packing than finer silica aerogel, indirectly generating more interparticle pores in the geopolymer matrix. The AG5-10 sample with a mixed silica aerogel recipe shows density in the middle of all aerogel samples. This can be explained simply by the mixing of the four silica aerogels as shown in Fig. 5 (e). The hypothesis of optimal packing of silica aerogel does not apply in AG5-10.

The skeleton density is related to the inherent properties of the raw materials. The skeleton density measured by the pycnometer is almost the same for all GFAR, which is due to the fact that all the raw materials used are fly ash and silica aerogel. Therefore, the skeleton density is in the range of 2308 kg/m^3 to 2350 kg/m^3, with very small deviations.

The porosity is calculated according to the dry bulk density and skeleton density. As presented in Fig. 6. The lowest porosity is 62.25%, obtained from the plain geopolymer foam concrete. However, the porosity is only slightly improved for the AG1-10, the finest aerogel powder, reaching 62.68%. This result indicates that IC3100 has no obvious effect on the improvement of the total porosity of GFAR. This could be attributed to the fact that the IC3100 aerogel is too small to support the air voids generated by the foaming agent and the surfactant mix. In the presence of surfactants, the hydrophobic silica aerogel particles will tend to be in the non-aqueous phase, which in this case is the gas phase (air) in the pores, thus the hydrophobic solid particles (silica aerogel) remain attached to the air-water contact surface [48]. Furthermore, the hydrophobic attraction [49] due to the van der Waals forces in an air-water-air system [50] will enhance this activity. As a result, the molecules can cluster in the air-containing pores. According to Wang et al. [51], hydrophobic particles stay in contact with the air bubble for a long period. As a result, the silica aerogel particles are likely to remain in close contact with the air bubble, and once the paste reaches the initial setting time, the particles are entrapped in the structure, making the further movement of particles impossible. This mechanism could explain why big particles are found close to the pores, reinforcing their structure and playing the role of the skeleton of the gas phase (air) trapped in the liquid phase (paste). Moreover, by adding a part of the larger aerogel particles instead of finer aerogel powder, good formability can be obtained as demonstrated in Ref. [52]. Another finding is that the bulk density for AG4-10 is the lowest, suggesting the large silica aerogel particles can increase the porosity of GFAR, achieving a porosity of 69.6%. Therefore, the silica aerogel with a large grain size plays a

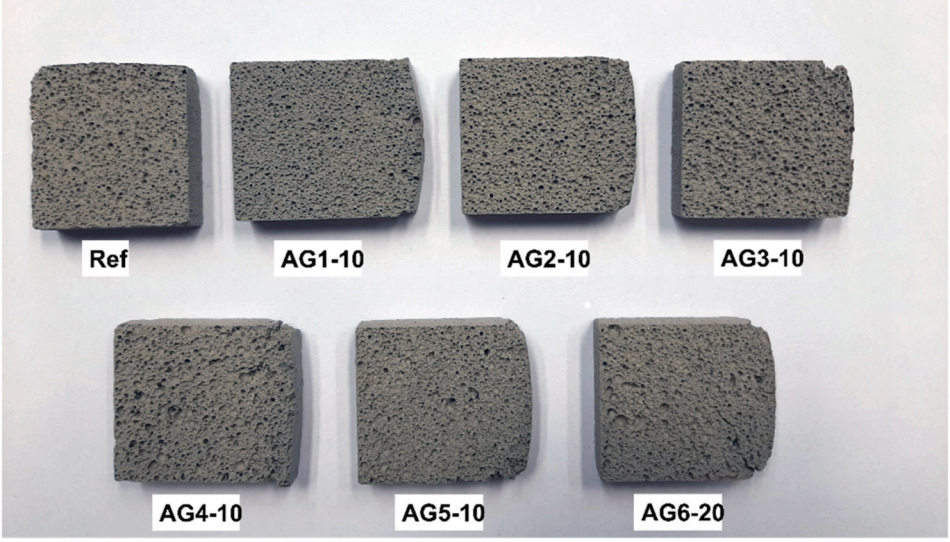

Fig. 4. Material samples examined during the investigation.

better role to create the porous structure of geopolymer foam concrete. It is demonstrated that the most porous structure can be achieved by the addition of the large grain size silica aerogel and increased concentration. To be specific, the 700–4000 μm silica aerogel has the best pore generation for GFAR.

The compressive strength of GFAR at 28 days is presented in Fig. 6. The reference sample has a compressive strength of 2.52 MPa. With the addition of silica aerogel, the samples show lower strength as expected, which is attributed to the low strength of silica aerogel (10–100 kPa) [9]. The strength of the AG1-10 sample is similar to the reference, so the finest silica aerogel has limited influence on the mechanical performance. However, the AG2-10, AG3-10, AG4-10 and AG5-10 have a higher reduction in compressive strength, reaching 1.84 MPa, 1.58 MPa, 1.49 MPa and 1.50 MPa, respectively. This result can be explained by the total porosity of the GFAR as discussed above. As expected, the 20% dosage aerogel sample AG6-20 has the lowest strength, however, due to the porous structure, it could have a better insulation performance. Another aspect is the weak bonding between the paste and the filler (silica aerogel particles), which can be seen in AG4-10 and AG6-20 which possess similar pore volumes, but 20% replacement is more detrimental to structural strength than 10% AG replacement.

3.2. Microstructural analysis

3.2.1. Optical image analysis

Fig. 7 shows an optical image of a cross-section of AG5-10, which is valuable for observing macropores and macrostructure. Many open channels can be observed in the geopolymer matrix (Fig. 7 (a)). Although the smallest silica aerogel particles are not detectable, it is presumed that they are incorporated in the matrix of the geopolymer solid network, reducing the solid thermal conductivity. Furthermore, as depicted in Fig. 7 (b), the pores are interconnected, and the matrix contains a silica aerogel particle. Fig. 7 (c) illustrates a large-sized silica aerogel embedded in a matrix, which belongs to LA1000 silica aerogel and may act as a thermal barrier and absorbent for acoustic waves, as well as providing a link and backbone between the air voids, finally increasing the acoustic absorption. The bigger pores around 100–700 μm are created to be cavities and openings, which contribute to the sound wave energy loss and friction. However, the small pores below 100 μm are more likely to remain closed, which can contribute to the thermal insulation of GFAR.

3.2.2. Micro-CT analysis

The software IPLFE v1.16 (Scanco Medical AG, Switzerland) is used to analyze the pore distribution of the developed composites on a 3D slice view. The pixel intensity is related to the density of the object, making it possible to separate the surrounding air, air voids and aerogel particles from the denser matrix. However, the density difference between air and silica aerogel is small, making the distinguishment between air and aerogel rather difficult.

A distance transformation is applied [53] which enables the collection of the data in the 3D visualisation form in a 3D model of the sample. The empty region surrounding the geopolymer is turned into a solid by filling. Following the identification of all pores on the surface and inside the prescribed contour, the pores are coloured differently depending on the size of the examined pore/particle [54]. It is able to generate a 3D-pore shape visualisation in all geopolymer renderings using the data gathered in this way on both the distribution and size of the pores (Fig. 8). Noteworthy, as mentioned in the methodology, micro-CT covers the pores above 10 μm which provides limitations related to small size pores. The pore size is divided into the groups related to the silica aerogel particles used in order to see the variations between samples, as well as the values, are normalized to 100 vol % (Fig. 9). The porosity below the detection threshold (10 μm) is calculated using the porosity estimated by the μCT and pycnometer technique, as shown in Table 7. A more detailed pore size distribution graph is referred to Fig. S1 (supplementary information).

The goal of the porosity distribution analysis is to check how silica aerogel particles affect the pore size distribution of GFAR. The size of the silica aerogel particles is used to establish the prescribed intervals in order to observe their possible impact on the pore size, which is also related to the presence of these particles in the matrix (Fig. 8). As can be observed, tiny particles have a minor influence on the matrix, but particles size ranging from 100 μm to 1200 μm enrich the structure with voids of various sizes, which contribute favourably to both in terms of thermal insulation and acoustic absorption, as evidenced by the AG3-10 (Table 7). Empty gaps with a restricted range of sizes are undesirable because they influence the material's acoustic and strength characteristics. The size and distribution of pores in the materials are depicted in Fig. 9, where the order of magnitude has been standardized in the form of a colour scale, allowing for comparing the matrices obtained. As can be seen, adding a particle with a size of up to 40 μm enriches the mixture with numerous fine air/silica aerogel gaps. As the particle size increases, the number of bigger components equally dispersed throughout the structure increases as well. Due to the presence of a big size fraction of

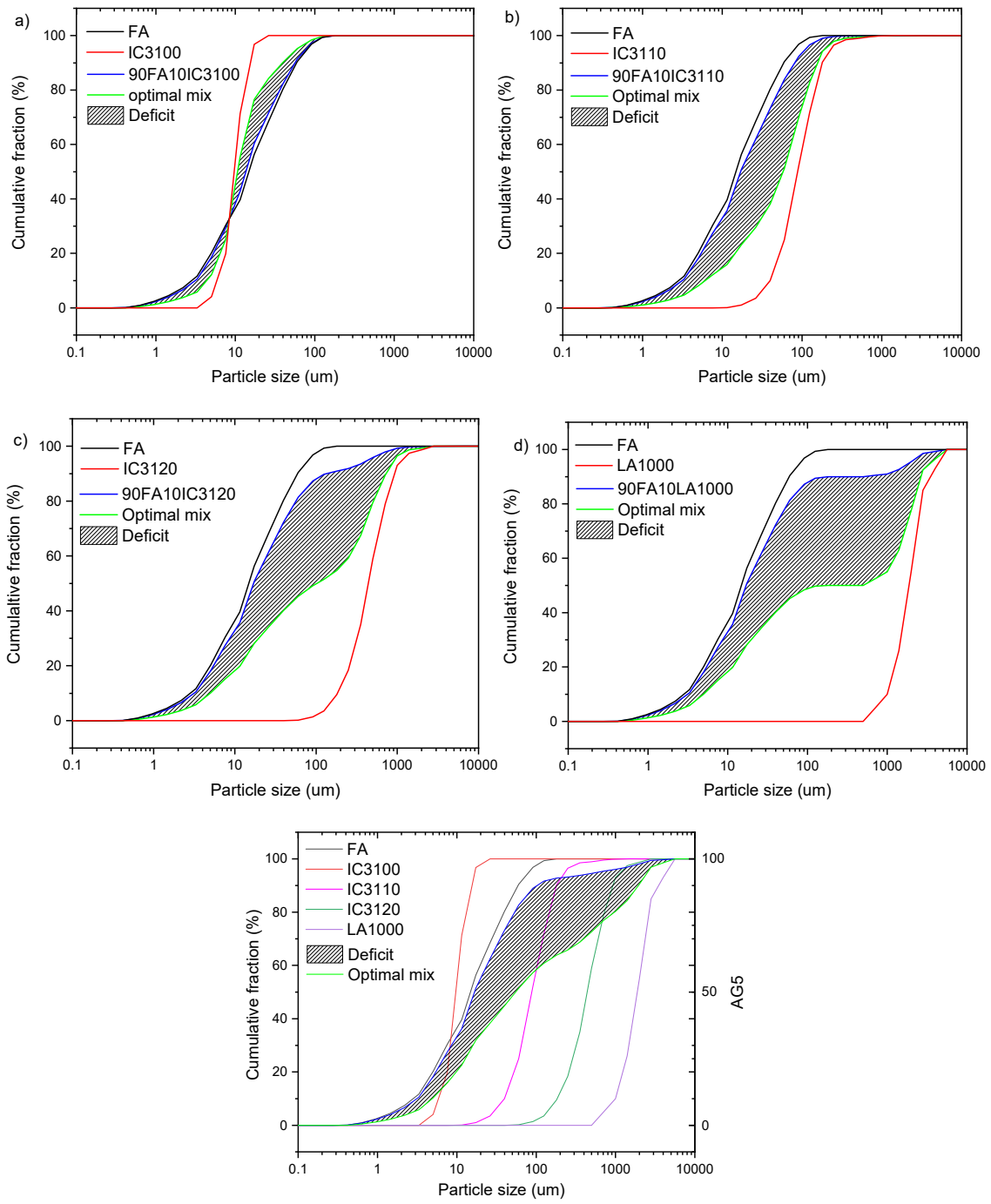

Fig. 5. The difference between the optimal mix curve and the actual curve of the mix from AG1-10 to AG5-10.

silica aerogel, AG4-10 contains many open spaces with a dimension of above 1 mm, which can let more sound get into the inner part of GFAR easily.

Moreover, Fig. 9 reveals that the contribution of small size pores is diminished by large particles. AG1-10 has the largest percentage of pores in the range of 10–50 μm (3% in normalized ranges to 100%), which is connected to silica aerogel particle size. Nevertheless, the impact of these particles can also be seen in AG5-10 and AG6-20, whose matrix contains particles of varied sizes. The pores above 700 μm have a considerable advantage for the LA1000 particles, which have a size range of 700–4000 μm. This has the largest influence on the pore size distribution in the case of AG4-10 which results in a reduced compressive strength when compared to other mixes enriched by 10% of silica aerogel. The pore structure of the AG5-10 mixed system is comparable to that of the AG4-10. However, in AG4-10 a reduced fraction of the smaller pores are observed, which is also owing to the existence of 2–40 μm particles in the mixed sample. Noteworthy, the distribution of pores in the AG2-10 material is not strictly determined by the size of the particles, only a 7% reduction of pores below 10 μm is observed.

The open porosity of GFAR calculated from μCT is presented in Table 8. The open porosity is important in determining the acoustic absorption of GFAR. The open porosity increases with the increasing particle size and concentration of silica aerogels. During the pore separation process, the resulting void spaces are examined for connection to identify individual objects, their volume, as well as connectivity [53]. After that, disconnected pores are separated from the linked pores in a

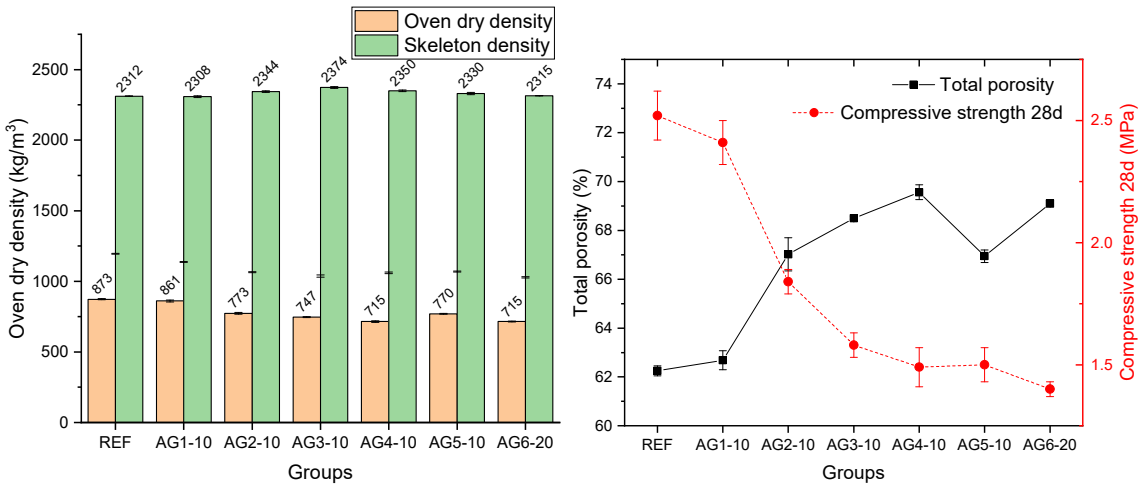

Fig. 6. Bulk density, skeleton density, total porosity and strength of the GFAR.

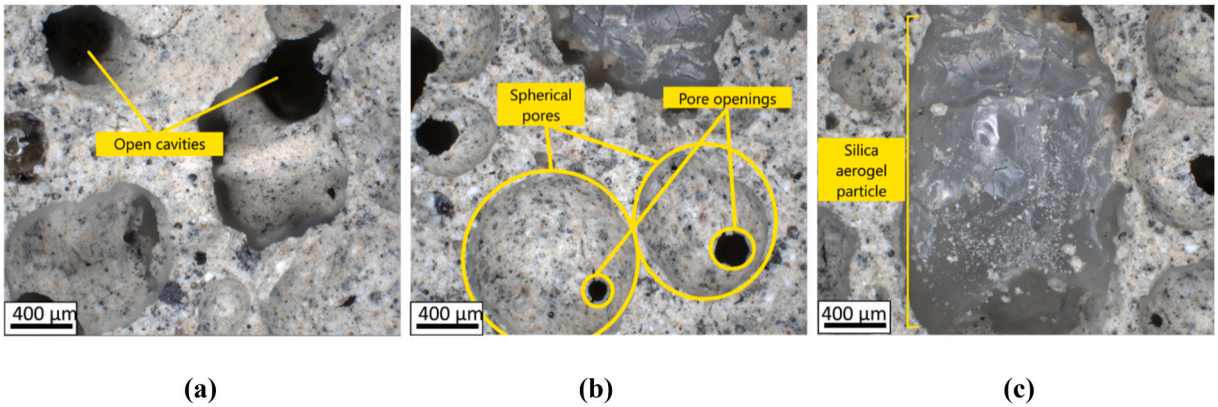

Fig. 7. Optical images of the cross-section of AG5-10.

3D representation, as shown in Fig. S2 (supplementary materials). A detailed evaluation of the closed pore visualisation can be found in the supplementary section.

3.2.3. UPV analysis

The UPV test of GFAR was carried out to evaluate the internal voids inside the samples. The results are shown in Table 9. The reference sample presents the highest speed to cross the sample, suggesting a more compacted structure than other groups. AG1-10 shows fewer voids or pores inside the structure than other samples with 10% silica aerogel, which is in accordance with the porosity results. However, the AG4-10 sample with the largest grain of silica aerogel shows the second-high speed among the 10% silica aerogel samples, contradicting the porosity results. Therefore, the large grains of silica aerogel mainly exist in the pores of the GFAR rather than in the solid network of geopolymer, resulting in a high velocity. While the finer silica aerogels are mainly positioned inside the geopolymer matrix, resulting in a slow velocity of sound. It has been expected that the AG6-20 shows the lowest speed of sound, suggesting the most porous structure of GFAR. While AG5-10 is still in the middle of the 4 samples with 10% silica aerogel, indicating the silica aerogel with mixed particle size has no obvious effect on the pore structure of GFAR.

3.3. Thermal conductivity of GFAR

3.3.1. Thermal conductivity at 100% dry condition

The thermal properties of the GFAR with different particle size of silica aerogel are presented in Fig. 10. The reference sample shows the highest thermal conductivity of 0.173 W/(m·K). The AG1-10 sample shows a slight reduction in thermal conductivity. With the increasing particle size of silica aerogel, the GFAR shows a lower thermal conductivity. The lowest thermal conductivity achieves 0.143 and 0.144 W/(m·K) for the AG3-10 and AG4-10 samples. On the other hand, the 20% silica aerogel AG6-20 shows the best thermal insulation, reaching 0.133 W/(m·K). This indicates the incorporation of more silica aerogel can decrease the thermal conductivity of GFAR as expected. The silica aerogel plays a role as an insulating filler with ultra-low thermal conductivity in the geopolymer matrix, thus reducing the thermal conductivity of all GFAR samples.

The effect of silica aerogel with different particle sizes on the thermal properties of GFAR can be attributed to two aspects. Firstly, large silica aerogel particles can create more inter-particle pores in the geopolymer matrix as discussed in Section 3.2. The thermal insulation of GFAR is closely related to the total porosity of the foam geopolymer. As can be referred in Fig. 6, the total porosity for AG4-10 and AG3-10 are higher than those of AG1-10 and REF. This factor can influence the thermal properties of GFAR as less heat was transported through solid, i.e. less solid conductivity is contributed to the total effective thermal conductivity of GFAR.

On the other hand, the influence of particle size on the thermal performance of GFAR mainly comes from the interfacial thermal resistance (ITR) of silica aerogel. Generally, finer silica aerogel has more interfacial area than coarser silica aerogel, due to the higher surface area of the small particles. Therefore, it is hypothesized that finer silica

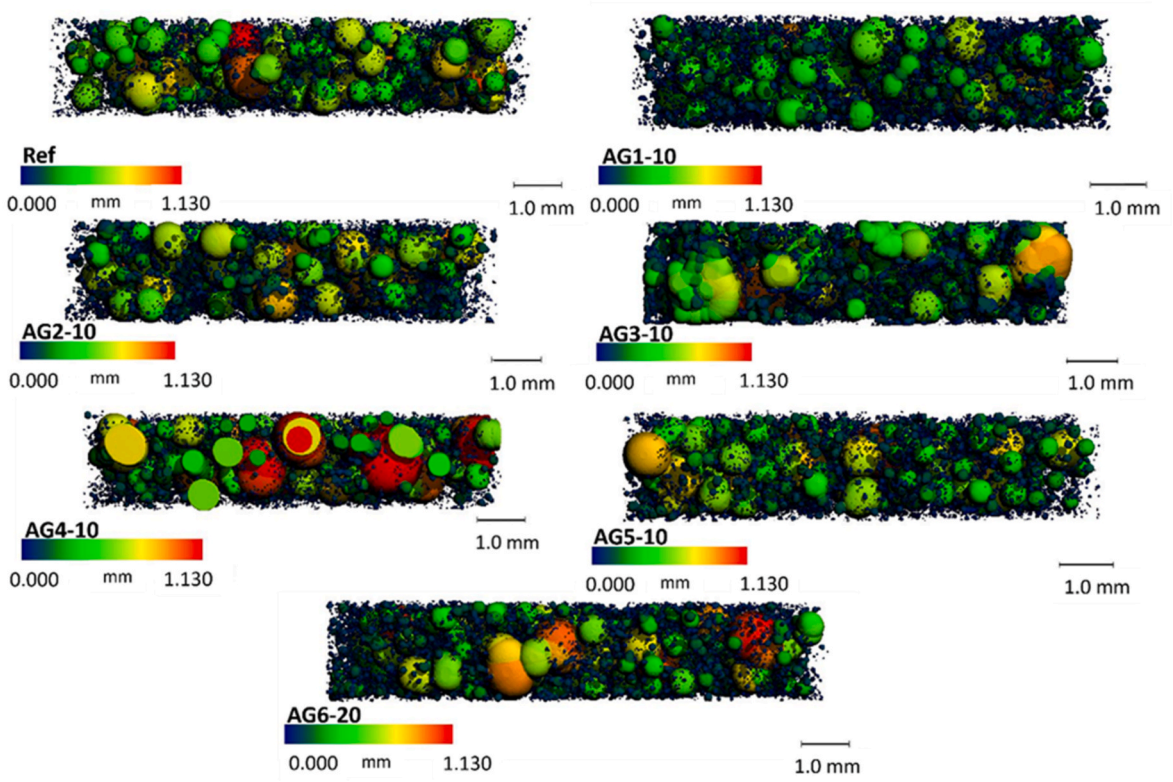

Fig. 8. Isolated air voids and silica aerogel particles system.

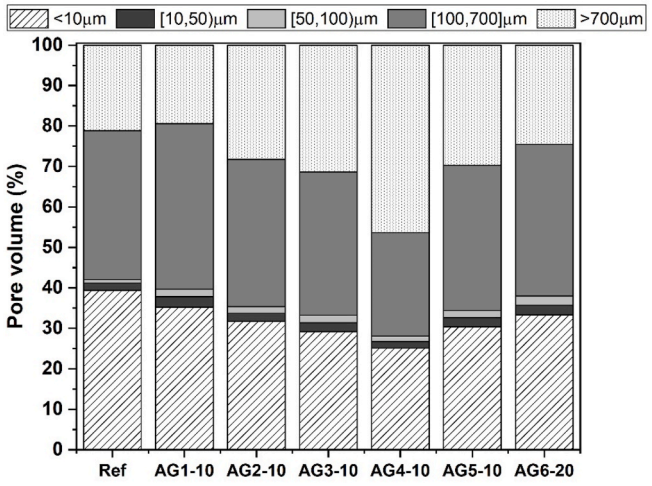

Fig. 9. Pore size distribution of GFAR retrieved from μCT and total porosity (normalized to 100%).

aerogel should have a higher interfacial thermal resistance than larger aerogel particles, assuming that the interfacial area obtains a lower thermal conductivity because it mainly consists of low-density geopolymer or air. However, in this study, it is found that the AG1-10 and AG2-10 have no obvious improvement in the thermal insulation of GFAR. It indicates that the ITR is not a decisive factor that influences the thermal conductivity in this case. The reason could be attributed to the fact that the thermal conductivity of interfacial area is even higher than silica aerogel, which is not the case compared to the previous study [55], where the ZnS/diamond composites show a lower thermal conductivity when a finer diamond is incorporated. Therefore, it is demonstrated that the particle size of silica aerogel mainly influences the total porosity of

Table 7
Pore size distribution retrieved by μCT and total porosity measurement.

	Overall porosity (%)	Pore volume in the range (μm)				
		<10	[10,50)	[50,100)	[100,700]	>700
Ref	62.3	24.5	1.1	0.5	23.0	13.1
AG1-10	62.7	22.1	1.6	1.1	25.6	12.2
AG2-10	67.0	21.2	1.4	1.0	24.4	18.9
AG3-10	68.5	20.0	1.5	1.3	24.3	21.5
AG4-10	69.6	17.5	1.1	0.9	17.8	32.2
AG5-10	66.9	20.3	1.5	1.2	24.0	19.9
AG6-20	69.1	23.0	1.7	1.6	25.9	16.9

Table 8
Open porosity of GFAR calculated from μCT.

Sample code	REF	AG1-10	AG2-10	AG3-10	AG4-10	AG5-10	AG6-20
Open porosity vol. %	36.6	37.2	44.2	47.2	46.8	44.4	47.1

Table 9
UPV test of GFAR.

Groups	Ref	AG1-10	AG2-10	AG3-10	AG4-10	AG5-10	AG6-20
Speed (m/s)	1447 ± 11	999 ± 6	745 ± 9	860 ± 3	970 ± 5	894 ± 8	756 ± 4
Time (s)	69.4	100.1	133.9	116.3	103.3	111.8	132.2

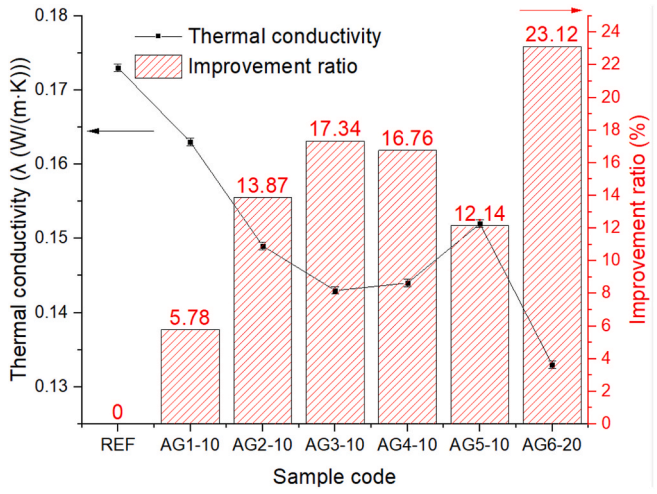

Fig. 10. Thermal conductivity and improvement ratio of the prepared GFARs.

GFAR while the interfacial thermal resistance is not significant.

Overall, the thermal conductivity is reduced with the increasing concentration of silica aerogel, thanks to the superior thermal insulation of silica aerogel. Although finer silica aerogel has a larger contacted interfacial area with geopolymer, the ITR is not a decisive factor for GFAR in this study. Therefore, the larger particle size of aerogel can even function better as a thermal insulator in the geopolymer foam concrete, due to the creation of more interparticle pores, increased total porosity, and also the optimized distribution and stability of the pores in the matrix.

The thermal conductivity versus the density and compressive strength versus thermal conductivity of building materials with the addition of silica aerogel particles are shown in Fig. 11 (a) and **(b)**. Compared with the GFAR prepared in this study, other materials with silica aerogel have higher thermal conductivities. The UHPC aerogel concrete obtains similar thermal conductivity, but the silica aerogel loading is much higher, replacing 70% of the natural aggregate. Cement-based aerogel foam concrete has a lower density, showing a linear trend as the silica aerogel dosage increased from 20% to 70%. The thermal conductivity decreases from 0.164 to 0.07 W/(m·K). Cement aerogel render shows a higher thermal conductivity at the same density range as GFAR. Also, the AIC (aerogel incorporated concrete) obtains higher density because coarse aggregate is used, showing a linear trend as well. Alkali-activated fly ash/slag concrete with silica aerogel has an even higher thermal conductivity than AIC, mainly because the used sand is much more conductive compared to the replaced aerogel. Cement aerogel mortar coating has a higher density and thermal conductivity. It is noteworthy that the GFAR has the lowest thermal conductivity in the specific density range compared to other aerogel incorporated samples. Thanks to the enhanced insulating properties of GFAR, it can be applied in certain building applications with thinner solutions, for instance, in building retrofit to increase the energy efficiency, especially considering the increased awareness of environmental impact caused by buildings.

The comparison of compressive strength with other aerogel incorporated materials is shown in Fig. 11 (b). It is noteworthy that the compressive strength of GFAR is only slightly lower than UHPC aerogel concrete. This is mainly because the UHPC recipe has a very low water to binder ratio of 0.20–0.25 and a better packing of the mixtures. For other materials with the addition of silica aerogel, the compressive strength is lower, which is attributed to the higher loading of silica aerogel to 50%, resulting in a lower strength. For the GFAR, the aerogel loading is only 10%, while can still reach a lower thermal conductivity. Therefore, the optimized geopolymer foam matrix plays an important role. The less silica aerogel in the matrix, the fewer defects in the interface of materials could have, thus leading to the higher compressive strength of GFAR.

3.3.2. *Water uptake and the effect on thermal conductivity*

The water uptake of GFAR at various humidity levels up to 80% and its effect on thermal conductivity is shown in Fig. 12. The water uptake of the reference sample is the highest, reaching 6.52%. This higher water uptake causes a significant rise in thermal conductivity, which shows a rise to 0.214 W/(m·K), increasing by 23.6% compared to the sample under 100% dry conditions. As can be observed, the silica aerogel incorporated samples show lower water uptake from AG1-10 to AG5-10. This is attributed to the hydrophobic nature of silica aerogel, as shown in the water contact angle image in Fig. 1 (c). As a result, the aerogel incorporated GFAR all have a smaller rise in thermal conductivity.

Different concentrations of silica aerogel show different levels of reduction in the water uptake of GFAR. Despite its extremely high total porosity, a sample containing 20 vol% silica aerogel (AG6-20) improves hygrothermal parameters significantly over the entire analyzed humidity range. The material has a low initial heat conductivity, and the influence of particles on the decrease of the absorbed water content at high humidity environment has also been revealed. Fig. 12 (d) may be used to analyze the negative effect of water on the degradation of thermal insulation qualities by taking into consideration as a starting value the effective thermal conductivity particular for a certain composite. The unfavourable effects of exposing the porous composite to high humidity conditions were decreased by enriching the geopolymer mix with 20% of silica aerogel. Therefore, it is concluded that more silica aerogel dosage in GFAR could have a significant positive effect on the

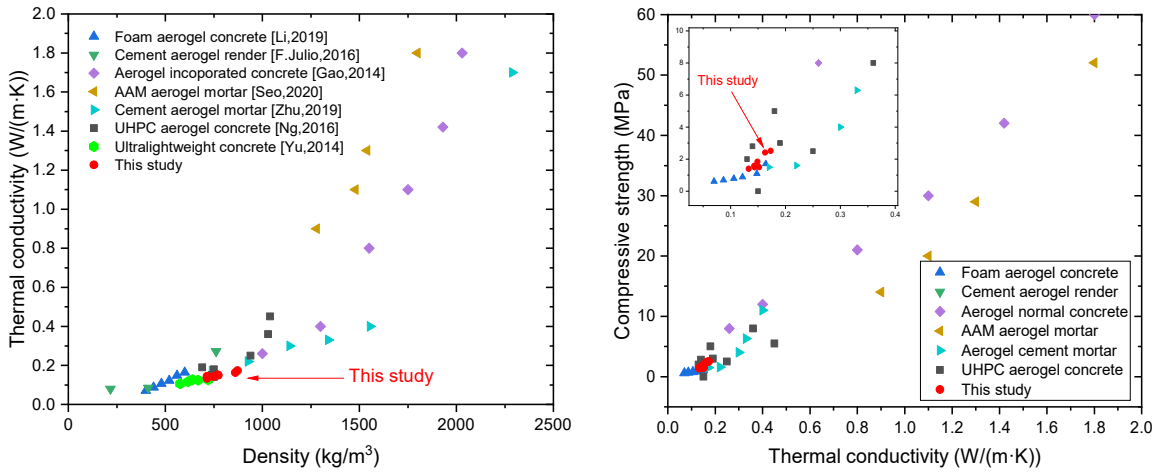

Fig. 11. (a) Thermal conductivity vs density (b) Compressive strength vs thermal conductivity of GFAR with other aerogel incorporated building materials.

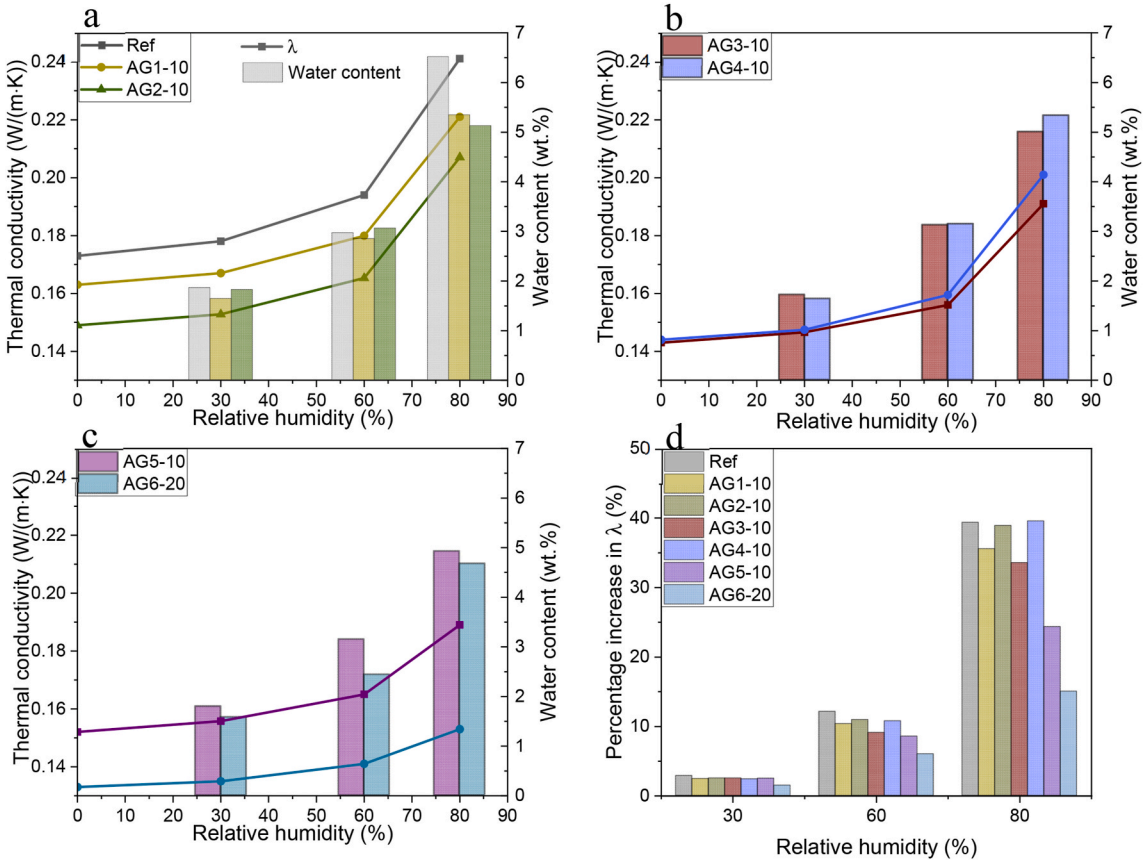

Fig. 12. Effective thermal conductivity and water content as a function of relative humidity.

thermal conductivity in a high humidity environment.

The water uptake at RH 80% of samples with 10 vol% replacement varies between 4.93% and 5.35%, thus the rise in thermal conductivity of GFAR is similar (Fig. 12d). Among these groups of GFAR, the AG5-10 and AG3-10 have a better performance than other groups in terms of increment in thermal conductivity. This increase in hygrothermal insulation could be owing to the much higher range of particle size from 100 μm to 1200 μm. It can be observed the mixing particles could have a positive effect on the hygrothermal performance than the narrow pore size distribution particles like AG1-10. The reason for this phenomenon could be considered in two aspects. Firstly, the finer silica aerogel has a higher hydrophobic surface area that can resist water from transportation as discussed in the previous section. The interfacial water resistance could be directly related to the water resistance of GFAR. Hence, the much finer silica aerogel could result in a more hydrophobic surface site in the matrix. Thus, the AG4-10 with the largest particle shows a worse performance in water uptake and increment in thermal conductivity. Secondly, the tortuosity of water transport is enhanced by adding smaller silica aerogel particles, because of the more hydrophobic positions in the matrix that spread evenly. With a wide range of silica aerogel particles, the packing of the silica aerogel becomes better and thus more channels for water transport are blocked by aerogels.

However, the AG1-10 sample shows a less effective contribution to thermal properties. The reason is the narrow particle size distribution of IC3100 from 10 to 40 μm that cannot effectively increase the tortuosity of moisture transport. It is demonstrated the addition of randomly distributed graphene particles can enhance the tortuosity and decrease the chloride transport in both concrete and mortar [56,57]. Therefore, a wider range of silica aerogel particles could improve the tortuosity better than IC3100 and LA1000, as can be reflected by the AG5-10, where the random particle size strategy also performs better in this case.

Additionally, the porosity, pore distribution and presence of cavities within the composite are examined in the group of GFAR enhanced with 10% aerogel. First and foremost, the significant difference in porosity (Fig. 4) between AG1-10 (62.7%) and AG2-10 (67.0%) is noted, since this is a critical aspect of the water transport mechanism in the pore structure, as evidenced by the decreased water absorption for RH30% and RH60% compared to AG2-10 (Fig. 9a). In the case of RH80%, however, it demonstrates the above-mentioned significance of silica aerogel particles in the water transport retardation. The reference sample, which has a similar total porosity and open-pore volume, has a lower resistance to water sorption than AG1-10.

When comparing materials with various pore size distributions (Fig. 9), such as AG3-10 and AG4-10 (Fig. 12 (b)), the phenomena of enhanced moisture sorption in the low humidity region through capillary suction is demonstrated. This implies that small pores are filled initially, and as the air humidity rises, larger pores are filled with several monolayers of water. The increased permeability of the composite, which can be measured using the open porosity metric (Table 8), intensifies this effect. The hygrothermal parameters are thus defined by the overlaying of two phenomena, namely the pore structure and superior characteristics of silica aerogel. Because of the excellent hygrothermal properties and relatively low cost owing to the use of low percentage aerogel, geopolymer foam aerogel render could be applied as an excellent interlayer for housing in a humid area. It can be considered as a multifunctional retrofit solution, especially for historic residential buildings where humidity control is crucial in high humidity areas, thanks to its low water absorption and constant insulation properties under high humidities.

3.4. Acoustic absorption

The acoustic absorption coefficient of GFAR with different dosages and particle size of silica aerogel are shown in Fig. 13. Due to the normal

incidence absorption coefficient varies with thickness, the value evaluated in this study for 20 mm and 50 mm are provided. The initial peak of the absorption curve moves to lower frequencies as the thickness of the sample grows, as predicted, due to the increasing tortuosity of the thicker samples [17]. Average values of the coefficient of absorption (α_{med}) of GFAR with different thickness are presented in Fig. 14. The reference sample presents a relatively low acoustic absorption efficiency, reaching an average coefficient of absorption (α_{med}) of 0.12 (50 mm) and 0.11 (20 mm). The maximum absorption occurs at 719 Hz with a coefficient of 0.37, which is typical for foamed concrete, whose efficiency is in the range of 0.13–0.50 over the frequency of 100–2000 Hz [58]. Noteworthy, samples enriched with silica aerogel, excluding AG1-10, exceed the maximum value of sound absorption coefficient (α_{max}: 0.56–0.79). With a 10% aerogel dosage in GFAR, the samples AG1-10, AG2-10, AG3-10 and AG4-10 all present higher acoustic absorption performance than the plain GFAR. The AG1-10 sample shows a slight increase in the acoustic absorption efficiency, with only an 8.1% increase in maximum efficiency, achieving 0.40 at a frequency of 759 Hz. The coefficient of absorption (α_{med}) increases to 0.29 (50 mm) and 0.21 (20 mm). The maximum acoustic absorption of AG2-10 also increases but is limited to 0.56 at a frequency of 468 Hz, with the coefficient of absorption (α_{med}) reaching 0.34 (50 mm) and 0.33 (20 mm). It indicates the finer silica aerogels only slightly increase the acoustic absorption. On the other hand, the AG3-10 and AG4-10 samples both increase the acoustic absorption to a much higher degree. The AG3-10 silica aerogel with 100–1200 μm particle size increases the max acoustic absorption to 0.63 at 444 Hz, while the largest rise happens for AG4-10, with an increase of 113.5% compared to plain geopolymer foam render, achieving 0.79 at a frequency of 505 Hz. Furthermore, the coefficient of absorption (α_{med}) of AG3-10 and AG4-10 increases to 0.47 and 0.44 for 50 mm samples, respectively. Therefore, the IC3120 and LA1000 could play a better role to improve the acoustic absorption of geopolymer foam composites.

The increase in silica aerogel dosage to 20% has a significant effect on the acoustic absorption efficiency, achieving the highest coefficient of absorption (α_{med}) of 0.51 for 50 mm sample. The 20% silica aerogel addition in GFAR can increase the maximum absorption to 0.78 at 666 Hz compared to the 10% addition of silica aerogel with mixed particle sizes, whose efficiency reaches 0.59 at 667 Hz. Therefore, the increase in the volume percentage of silica aerogel indeed increases the acoustic performance of GFAR.

The hypothesis of using silica aerogel with a mixed particle size to increase the acoustic absorption of GFAR is not proved in this study. The addition of silica aerogels with multi-scale sizes in GFAR can only be explained by a simple mixing mechanism. The acoustic absorption performance of AG5-10 is in the middle of the four GFAR samples with single aerogel addition. Therefore, it is suggested that the silica aerogel with a larger particle size could function better as an enhancer for improvement in acoustic properties, which is better than the much finer fraction of silica aerogel.

Detailed studies on the acoustic absorption of foam concrete are relatively rare. Compared to other kinds of foam concrete, the sound absorption of GFAR in this study is higher, and the range of coefficient above 0.5 is wider, from around 500 Hz–2500 Hz. The rise in acoustic absorption could be attributed to the higher open porosity and the inherent acoustic absorption of silica aerogel. As shown in Table 10, the acoustic absorption of other foam concretes presents different values at different frequencies. The foam concrete can be prepared with different methods, for instance, pre-foamed concrete and aerated autoclaved concrete. Zhang et al. [59] investigated the acoustic absorption of fly ash/slag geopolymer pre-foam concrete, which has a maximum coefficient of 0.8, but with a very narrow absorption peak at 40–150 Hz. Neithalath et al. [60] prepared foamed concrete samples and presented absorption coefficients in the range of 0.20–0.30 with a bulk density of 400–700 kg/m^3. However, the foam concrete prepared had a closed pore network, mitigating the sound propagation leading to reduced sound absorption. Therefore, it is also important to optimize the processing parameters, for instance, the optimal amount of foaming agent and surfactant, to make foam concrete with a much higher open porosity if the acoustic absorption property is desired. Thanks to the excellent acoustic absorption of the developed GFAR, it can reach a relatively high acoustic absorption performance compared to other foam plasters. The acoustic absorption coefficient of GFAR in this study increased around 5 times with only 10% volume of aerogel compared to reference sample, allowing a significant increase in sound absorption coefficiency. Hence, the developed GFAR can be applied as an supplementary sound absorber in the theatre to other porous materials like acoustic panels, considering its excellent thermal insualtion performance.

3.5. Proposed mechanism

The mechanism of the improved performance of GFAR with different silica aerogel can be described and schematically shown in Fig. 15. The proposed mechanism is that the larger silica aerogel can crosslink the porous structure generated by the foaming agent, forming more interconnected open pores in the GFAR, thus increasing the sound absorption performance. Meanwhile, the total porosity of GFAR is also higher with much bigger silica aerogel particles, thus the thermal insulation of GFAR is also improved. The contribution of finer silica aerogel to the thermal insulation and acoustic absorption of GFAR is limited. The small particle sizes of silica aerogel, mainly the IC3100 and IC3110 particles, are placed inside the geopolymer matrix. However, the silica aerogel particles are too small to provide support for air voids created by H_2O_2, thus most of the small particles cannot play the role of a bridge or support air voids. While the larger particle size of silica aerogel, mainly for IC3120 and LA1000, are linked to the pores of the GFAR and can increase the total porosity and open porosity. It should be noted that the open porosity of the prepared geopolymer is relatively higher than other kinds of geopolymer foam concrete. The TX-100/SDS surfactant mix has a synergistic effect in lowering surface tension [62,63], as well as increased foam generation capacity and stability [64,65]. Therefore, the number of interconnected pores is higher than other foam concrete.

Fig. 16 **(a)** depicts the relationship between thermal conductivity, sound absorption and total porosity for the samples which contain 10 vol % of silica aerogel (AG1-10 to AG5-10). There are two regions where the parameters of thermal insulation and acoustic absorption do not develop in lockstep with the total porosity. Therefore, both cases are examined to check whether pore size influences their performance. The first case (Fig. 16 (b)) investigates AG2-10 and AG5-10 which are characterized by similar total porosity. However, the thermal and acoustic performances are different. Case I demonstrates that the variation in porosity occurs exclusively in two pore size ranges (below 10 μm and above 700 μm). It can be shown that having a greater pore volume of a larger size is beneficial for acoustic characteristics [66] but pores below 10 μm of the AG2-10 sample favour thermal insulation.

The second case (Fig. 16 (c)) discusses an anomaly (AG3-10 and AG4-10) in which an increase in porosity does not result in an improvement in the thermal and acoustic properties. Apart from the predominant role of the volume of the pores, the values of these parameters are also influenced by their size, shape and the presence/absence of connections between the pores. It can be presumed that it is advantageous for the material that the distribution of pores is even as it is confirmed by case I, as well as AG4-10 in case II which the sample is distinguished by a majority of air voids larger than 700 μm and a decrease in the number of pores between 100 and 700 μm and less than 10 μm. Despite having a greater total porosity, AG4-10 has a slightly higher thermal conductivity. Indeed, this discrepancy might be disregarded, however, a drop in conductivity will be expected.

The observation from Case I, namely an insufficient number of small-size pores [67] and an unequal distribution of size in the cross-section of the sample, supports this phenomenon. Furthermore, bigger size voids have a higher likelihood of forming connections between them, which is

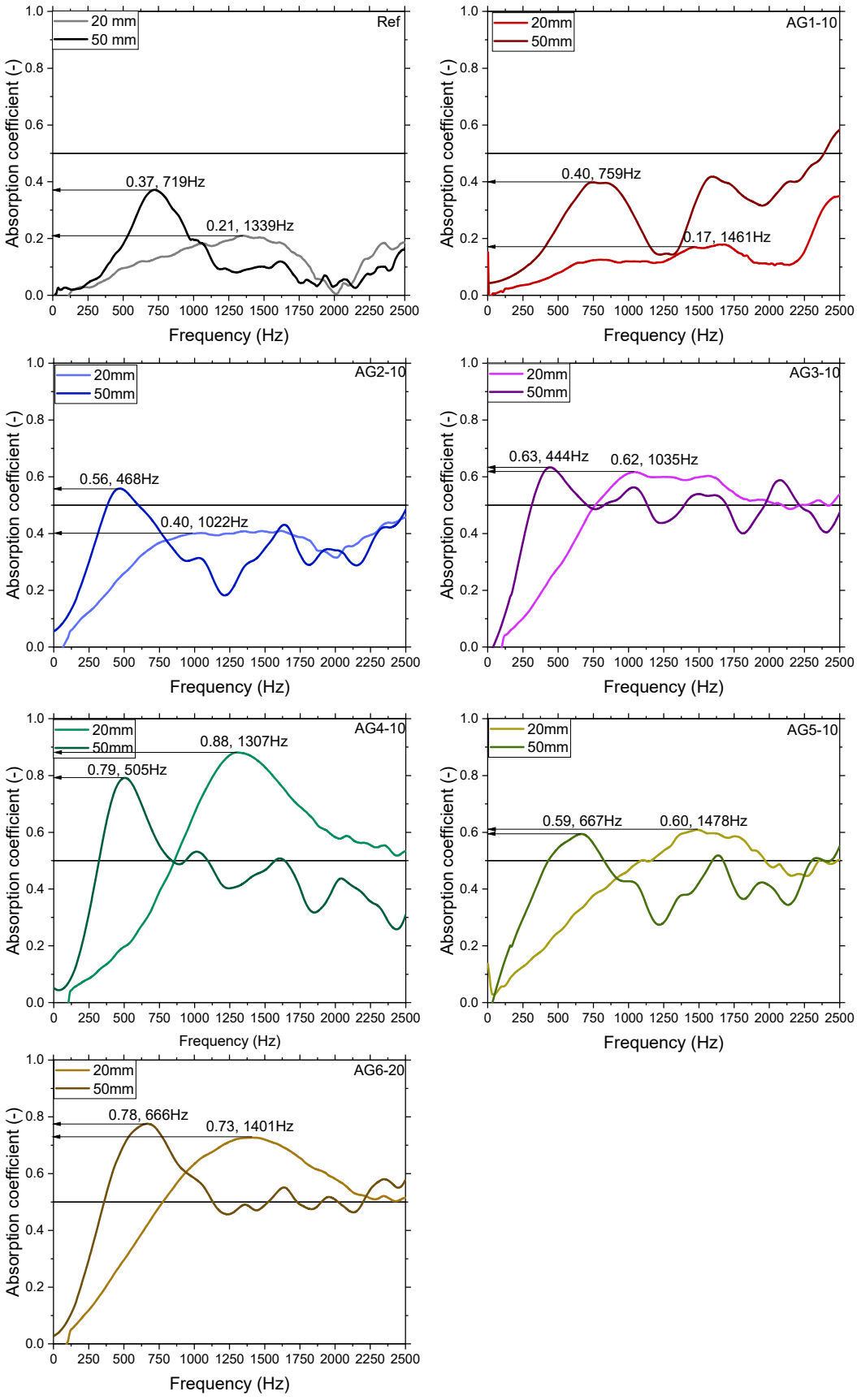

Fig. 13. Acoustic absorption of GFAR with different composite thickness, dosage and particle size of silica aerogel.

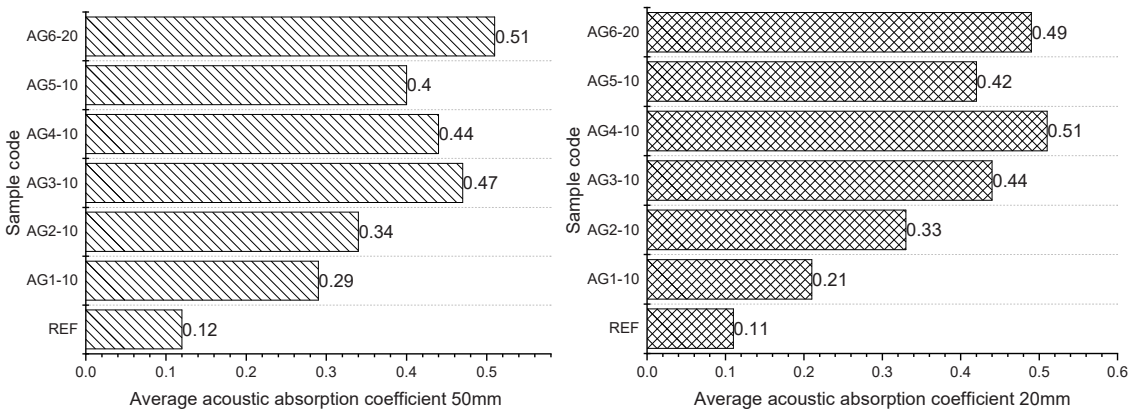

Fig. 14. Average values of the coefficient of absorption (α_{med}) of 50 mm and 20 mm GFAR samples.

Table 10
Acoustic absorption of different kinds of foam concrete.

Foam concretes	Maximum sound absorption coefficient	Peak frequency (Hz)	Density (kg/m^3)	Literature
Foam geopolymer concrete with aerogel	0.79	450–700	700–800	This study
Geopolymer foam concrete	0.8	40–150	600–1200	[59]
Aerated autoclaved concrete	0.12–0.36	–	250–500	[61]
Foamed cellular concrete	0.2–0.3	–	400–700	[60]

beneficial for the acoustic absorption of GFAR [60].

In summary, the large pore size beyond 700 μm is favourable for acoustic absorption but cannot be excessive. A moderate number of smaller pores less than 700 μm contribute to the air molecules vibrating and interacting with the pore walls, leading to the conversion of sound energy to heat and then dissipating. In terms of thermal insulation, the small pores less than 10 μm can be beneficial for the thermal insulation of GFAR.

4. Conclusions

The main objective of this study is to investigate the influence of the particle size of silica aerogel on the thermal and acoustic performance of foamed geopolymers. Parameters such as thermal conductivity, acoustic absorption and hygrothermal performance of GFAR are the main focus of this study. In addition, an insulation mechanism is proposed, and the following are its essential components:

- The total porosity of the geopolymer foam aerogel render is increased with the increasing particle size of aerogel. Moreover, the μ-CT analysis indicates the GFAR with larger silica aerogel particles has higher open porosity. The smaller silica aerogel can be spread in the solid network of geopolymer matrix, while the large silica aerogel can be positioned between the pores, thus providing additional openings.
- The acoustic absorption of the geopolymer foam aerogel render is much higher than the plain foam geopolymer render, which is contributed from the more open porosity in GFAR, and the inherent sound absorption of silica aerogel. The open porosity increases as the size of the aerogel increases. Moreover, silica aerogel with a larger particle size plays a better role to improve sound absorption due to providing a bridging effect between the air voids.
- The thermal insulation of GFAR is slightly improved with the addition of 10% silica aerogel. The thermal conductivity is firstly related

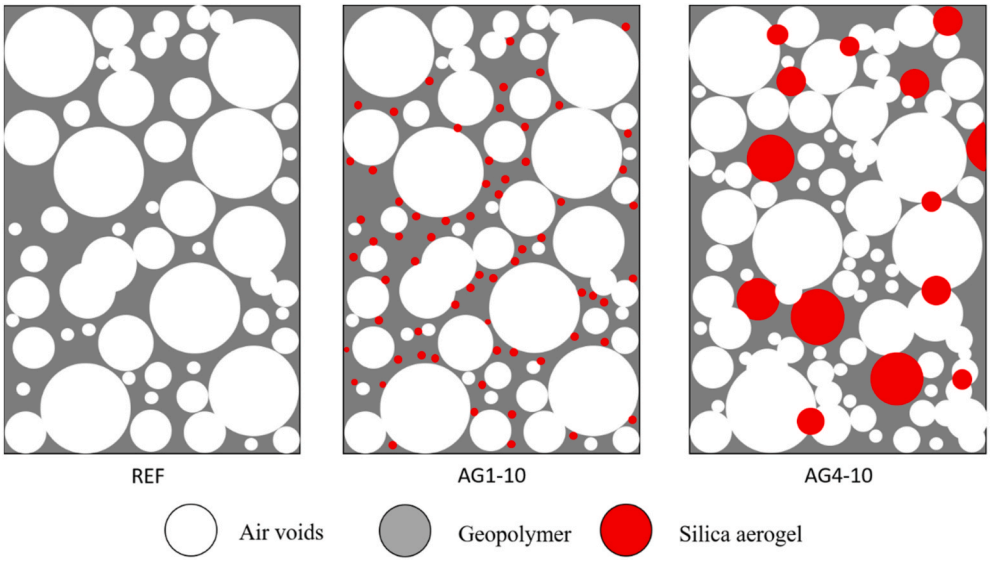

Fig. 15. Schematic illustration of GFAR microstructure.

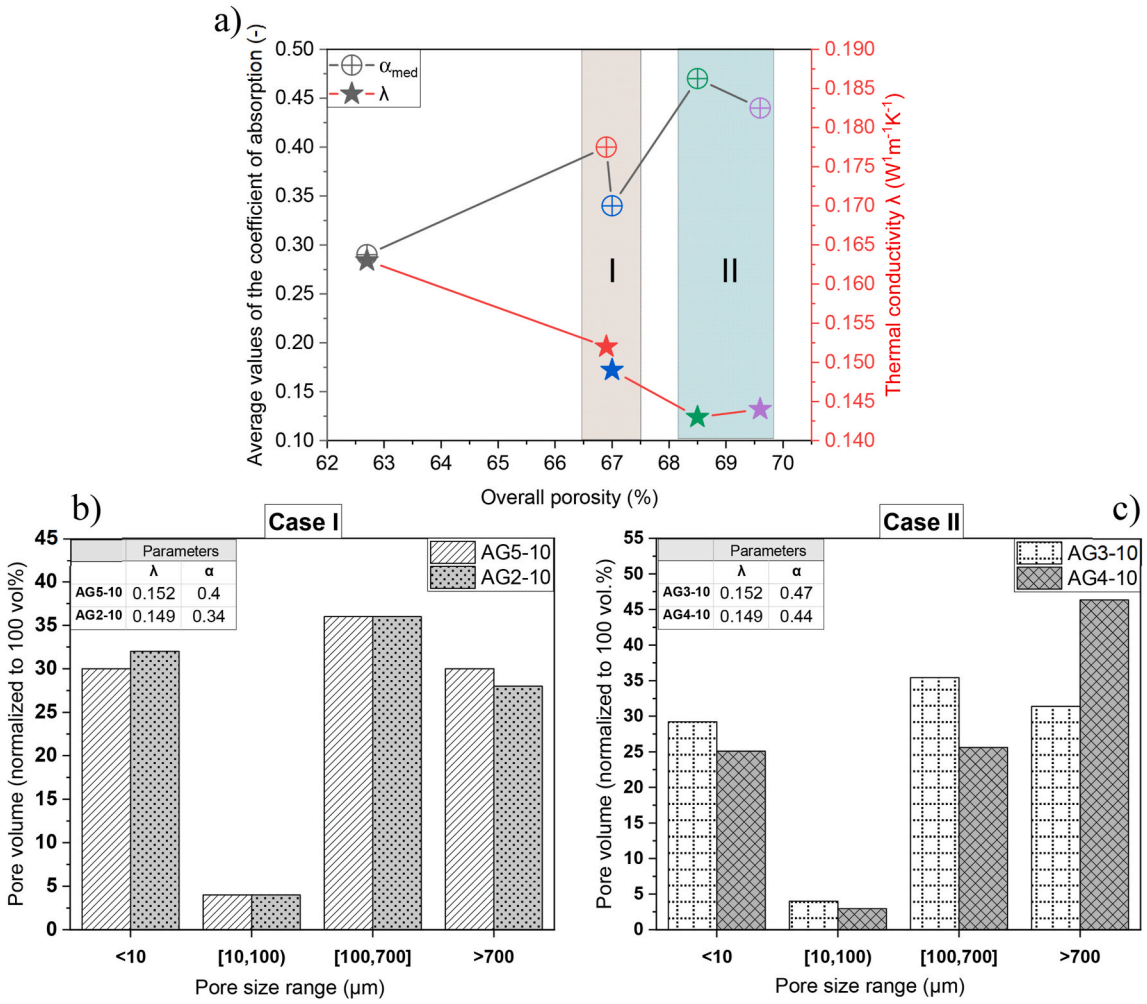

Fig. 16. Thermal conductivity and acoustic absorption - depending on porosity and pore size.

to the total porosity of GFAR. Secondly, the positive role of pores below 10 μm in reducing thermal conductivity is observed. The interfacial thermal resistance related to aerogel particles is not significant.

- The hygrothermal behaviour of 20 vol% silica aerogel enriched GFAR is significantly improved compared to the plain composite, demonstrated by the lower water uptake and thermal conductivity after conditioning to various humidities up to 80%. Among composites with 10 vol% replacement ratio, a wide range of smaller aerogel particles have a bigger influence, due to the more hydrophobic surface area and the tortuosity created that increases the moisture resistance of GFAR.
- In summary, the large pore size beyond 700 μm is favourable for acoustic waves entering the inner structure of GFAR. A moderate number of smaller pores less than 700 μm contribute to the vibration of air molecules and interaction with the pore walls, leading to the conversion of sound energy to heat and then dissipating. In terms of thermal insulation, small pores less than 10 μm can be beneficial for the thermal insulation of GFAR.

Declaration of competing interest

The authors declare that they have no known competing financial interests or personal relationships that could have appeared to influence the work reported in this paper.

Data availability

Data will be made available on request.

Acknowledgement

This research is supported by the National Natural Science Foundation of China (Grant No. 52178246), the Materials innovation institute M2i (www.m2i.nl) (Project No. S17013a), the Technology Foundation TTW (www.stw.nl), which is part of the Netherlands Organization for Scientific Research (www.nwo.nl). and Eindhoven University of Technology. Dr. Jieun Yang is acknowledged for the experimental support on acoustic absorption test.

Appendix A. Supplementary data

Supplementary data to this article can be found online at https://doi.org/10.1016/j.compositesb.2022.110048.

References

[1] Cao M, Liu B-W, Zhang L, Peng Z-C, Zhang Y-Y, Wang H, et al. Fully biomass-based aerogels with ultrahigh mechanical modulus, enhanced flame retardancy, and great thermal insulation applications. Compos B Eng 2021;225:109309.
[2] Nejat P, Jomehzadeh F, Taheri MM, Gohari M, Muhd MZ. A global review of energy consumption, CO2 emissions and policy in the residential sector (with an overview of the top ten CO2 emitting countries). Renew Sustain Energy Rev 2015;43:843–62. https://doi.org/10.1016/J.RSER.2014.11.066.

[3] Ikutegbe CA, Farid MM. Application of phase change material foam composites in the built environment: a critical review. Renew Sustain Energy Rev 2020;131:110008. https://doi.org/10.1016/J.RSER.2020.110008.

[4] Venegas R, Zieliński TG, Núñez G, Bécot F-X. Acoustics of porous composites. Compos B Eng 2021;220:109006.

[5] Pacheco Torgal F, Buratti C, Kalaiselvam S, Granqvist CG, Ivanov V. Nano and biotech based materials for energy building efficiency. 2016. https://doi.org/10.1007/978-3-319-27505-5.

[6] Chen YX, Wu F, Yu Q, Brouwers HJH. Bio-based ultra-lightweight concrete applying miscanthus fibers: acoustic absorption and thermal insulation. Cem Concr Compos 2020;114. https://doi.org/10.1016/j.cemconcomp.2020.103829.

[7] Sun J, Wu Z, An B, Ma C, Xu L, Zhang Z, et al. Thermal-insulating, flame-retardant and mechanically resistant aerogel based on bio-inspired tubular cellulose. Compos B Eng 2021;220:108997.

[8] Yang W-J, Wei C-X, Yuen ACY, Lin B, Yeoh GH, Lu H-D, et al. Fire-retarded nanocomposite aerogels for multifunctional applications: a review. Compos B Eng 2022:109866.

[9] Chen YX, Sepahvand S, Gauvin F, Schollbach K, Brouwers HJH, Yu Q. One-pot synthesis of monolithic silica-cellulose aerogel applying a sustainable sodium silicate precursor. Construct Build Mater 2021;293:123289. https://doi.org/10.1016/J.CONBUILDMAT.2021.123289.

[10] Madyan OA, Fan M, Feo L, Hui D. Enhancing mechanical properties of clay aerogel composites: an overview. Compos B Eng 2016;98:314–29. https://doi.org/10.1016/j.compositesb.2016.04.059.

[11] Wang Y, Liu X, Zhang W, Li Z, Zhang Y, Li Y, et al. Effects of Si/Al ratio on the efflorescence and properties of fly ash based geopolymer. J Clean Prod 2020;244:118852. https://doi.org/10.1016/j.jclepro.2019.118852.

[12] Ng S, Jelle BP, Sandberg LIC, Gao T, Wallevik ÓH. Experimental investigations of aerogel-incorporated ultra-high performance concrete. Construct Build Mater 2015;77:307–16. https://doi.org/10.1016/j.conbuildmat.2014.12.064.

[13] Gao T, Jelle BP, Gustavsen A, Jacobsen S. Aerogel-incorporated concrete: an experimental study. Construct Build Mater 2014;52:130–6. https://doi.org/10.1016/j.conbuildmat.2013.10.100.

[14] de Fátima Júlio M, Ilharco LM, Soares A, Flores-Colen I, de Brito J. Silica-based aerogels as aggregates for cement-based thermal renders. Cem Concr Compos 2016;72:309–18. https://doi.org/10.1016/j.cemconcomp.2016.06.013.

[15] Seo J, Bae SJ, Jang DI, Park S, Yang B, Lee HK. Thermal behavior of alkali-activated fly ash/slag with the addition of an aerogel as an aggregate replacement. Cem Concr Compos 2020;106:103462. https://doi.org/10.1016/j.cemconcomp.2019.103462.

[16] Zhu P, Brunner S, Zhao S, Griffa M, Leemann A, Toropovs N, et al. Study of physical properties and microstructure of aerogel-cement mortars for improving the fire safety of high-performance concrete linings in tunnels. Cem Concr Compos 2019;104:103414. https://doi.org/10.1016/j.cemconcomp.2019.103414.

[17] Buratti C, Merli F, Moretti E. Aerogel-based materials for building applications: influence of granule size on thermal and acoustic performance. Energy Build 2017;152:472–82.

[18] Buratti C, Moretti E, Belloni E, Agosti F. Development of innovative aerogel based plasters: preliminary thermal and acoustic performance evaluation. Sustain Times 2014;6:5839–52. https://doi.org/10.3390/su6095839.

[19] Spagnol S, Lartigue B, Trombe A, Gibiat V. Modeling of thermal conduction in granular silica aerogels. J Sol Gel Sci Technol 2008;48:40–6. https://doi.org/10.1007/s10971-008-1759-3.

[20] Ng S, Jelle BP, Zhen Y, Wallevik ÓH. Effect of storage and curing conditions at elevated temperatures on aerogel-incorporated mortar samples based on UHPC recipe. Construct Build Mater 2016;106:640–9. https://doi.org/10.1016/j.conbuildmat.2015.12.162.

[21] Pedroso M, Flores-Colen I, Silvestre JD, Gomes MG, Silva L, Ilharco L. Physical, mechanical, and microstructural characterisation of an innovative thermal insulating render incorporating silica aerogel. Energy Build 2020;211:109793. https://doi.org/10.1016/j.enbuild.2020.109793.

[22] Zhang CY, Han R, Yu B, Wei YM. Accounting process-related CO2 emissions from global cement production under Shared Socioeconomic Pathways. J Clean Prod 2018;184:451–65. https://doi.org/10.1016/J.JCLEPRO.2018.02.284.

[23] Lahoti M, Wijaya SF, Tan KH, Yang EH. Tailoring sodium-based fly ash geopolymers with variegated thermal performance. Cem Concr Compos 2020. https://doi.org/10.1016/j.cemconcomp.2019.103507.

[24] Zhao J, Tong L, Li B, Chen T, Wang C, Yang G, et al. Eco-friendly geopolymer materials: a review of performance improvement, potential application and sustainability assessment. J Clean Prod 2021:127085.

[25] Krotov O, Gromyko P, Gravit M, Sultanov S. Thermal conductivity of geopolymer concrete with different types of aggregate. In: Int. Sci. Conf. Energy, Environ. Constr. Eng. Springer; 2020. p. 296–303.

[26] Huang Y, Gong L, Pan Y, Li C, Zhou T, Cheng X. Facile construction of the aerogel/geopolymer composite with ultra-low thermal conductivity and high mechanical performance. RSC Adv 2018;8:2350–6.

[27] Dhasindrakrishna K, Pasupathy K, Ramakrishnan S, Sanjayan J. Progress, current thinking and challenges in geopolymer foam concrete technology. Cem Concr Compos 2021;116:103886.

[28] Masi G, Rickard WDA, Vickers L, Bignozzi MC, Van Riessen A. A comparison between different foaming methods for the synthesis of light weight geopolymers. Ceram Int 2014;40:13891–902. https://doi.org/10.1016/j.ceramint.2014.05.108.

[29] Bai C, Franchin G, Elsayed H, Zaggia A, Conte L, Li H, et al. High-porosity geopolymer foams with tailored porosity for thermal insulation and wastewater treatment. J Mater Res 2017;32:3251–9. https://doi.org/10.1557/jmr.2017.127.

[30] Tarameshloo A, Kani EN, Allahverdi A. Performance evaluation of foaming agents in cellular concrete based on foamed alkali-activated slag. Can J Civ Eng 2017;44:893–8.

[31] Samson G, Cyr M. Porous structure optimisation of flash-calcined metakaolin/fly ash geopolymer foam concrete. Eur J Environ. Civ Eng. 2018;22:1482–98.

[32] Yu Q, Li X, Wang Z, Xue J. Characterization and performance evaluation of metakaolin-based geopolymer foams obtained by adding palm olein as the foam stabilizer. Materials 2022;15:3570.

[33] Maia J, Pedroso M, Ramos NMM, Pereira PF, Flores-Colen I, Gomes MG, et al. Hygrothermal performance of a new thermal aerogel-based render under distinct climatic conditions. Energy Build 2021;243:111001. https://doi.org/10.1016/j.enbuild.2021.111001.

[34] Alioua T, Agoudjil B, Boudenne A, Benzarti K. Sensitivity analysis of transient heat and moisture transfer in a bio-based date palm concrete wall. Build Environ 2021;202:108019. https://doi.org/10.1016/j.buildenv.2021.108019.

[35] Ruan S, Chen S, Lu J, Zeng Q, Liu Y, Yan D. Waterproof geopolymer composites modified by hydrophobic particles and polydimethylsiloxane. Compos B Eng 2022;237:109865.

[36] Stahl T, Brunner S, Zimmermann M, Ghazi Wakili K. Thermo-hygric properties of a newly developed aerogel based insulation rendering for both exterior and interior applications. Energy Build 2012;44:114–7. https://doi.org/10.1016/j.enbuild.2011.09.041.

[37] Zhao C, Li Y, Ye W, Shen X, Yuan X, Ma C, et al. Performance regulation of silica aerogel powder synthesized by a two-step Sol-gel process with a fast ambient pressure drying route. J Non-Cryst Solids 2021;567:120923. https://doi.org/10.1016/j.jnoncrysol.2021.120923.

[38] Chen YX, Hendrix Y, Schollbach K, Brouwers HJH. A silica aerogel synthesized from olivine and its application as a photocatalytic support. Construct Build Mater 2020;248:118709. https://doi.org/10.1016/j.conbuildmat.2020.118709.

[39] Abdul Halim ZA, Mat Yajid MA, Idris MH, Hamdan H. Effects of silica aerogel particle sizes on the thermal–mechanical properties of silica aerogel–unsaturated polyester composites. Plast, Rubber Compos 2017;46:184–92.

[40] Kucharek M, MacRae W, Yang L. Investigation of the effects of silica aerogel particles on thermal and mechanical properties of epoxy composites. Composites Part A Appl Sci Manuf 2020;139:106108.

[41] Rickard WDA, Williams R, Temuujin J, Van Riessen A. Assessing the suitability of three Australian fly ashes as an aluminosilicate source for geopolymers in high temperature applications. Mater Sci Eng, A 2011;528:3390–7.

[42] EN 12390-7 BS. Testing hardened concrete Part 7: density of hardened concrete. J Chem Inf Model 2009;53:1689–99.

[43] EN1097-7. Test for mechanical and physical properties of aggregates-Part 7: determination of the particle density of filler-phcnometer method. 1999.

[44] Li X, Liu B, Wu Q. Enhanced low-frequency sound absorption of a porous layer mosaicked with perforated resonator. Polymers 2022;14:223.

[45] BS EN 196-1. Methods of testing cement. Part 1 determ strength. 2005.

[46] ASTM C 597-02. Pulse velocity through concrete. U. S. A Soc Test Mater 2003;4:3–6.

[47] Hygrothermal performance of building materials and products — determination of hygroscopic sorption properties. 2013. p. 1–22. Iso/Wd 12571 2010.

[48] Tansel B, Boglaienko D. Characterization of aggregation and declustering tendency of hydrophobic fine particles in water. Granul Matter 2019;21:1–12.

[49] Maestro A, Guzmán E. Colloids at fluid interfaces. Process, vol. 7; 2019. https://doi.org/10.3390/pr7120942.

[50] Tabor RF, Grieser F, Dagastine RR, Chan DYC. The hydrophobic force: measurements and methods. Phys Chem Chem Phys 2014;16:18065–75.

[51] Wang C, Liu Y, Xu L, Qiu M, Jiang H, Chen R. Rebound behaviors of hydrophilic particle on gas bubble: effect of particle size and liquid properties. J Chem Technol Biotechnol 2021.

[52] Li P, Wu H, Liu Y, Yang J, Fang Z, Lin B. Preparation and optimization of ultra-light and thermal insulative aerogel foam concrete. Construct Build Mater 2019;205:529–42. https://doi.org/10.1016/j.conbuildmat.2019.01.212.

[53] Landis EN, Corr DJ. Three dimensional analysis of air void systems in concrete. Meas. Monit. Model. Concr. Prop. Springer; 2007. p. 517–24. https://doi.org/10.1007/978-1-4020-5104-3_63.

[54] Korat L, Ducman V, Legat A, Mirtič B. Characterisation of the pore-forming process in lightweight aggregate based on silica sludge by means of X-ray micro-tomography (micro-CT) and mercury intrusion porosimetry (MIP). Ceram Int 2013;39:6997–7005.

[55] Every AG, Tzou Y, Hasselman DPH, Raj R. The effect of particle size on the thermal conductivity of ZnS/diamond composites. Acta Metall Mater 1992;40:123–9. https://doi.org/10.1016/0956-7151(92)90205-S.

[56] Du H, Pang SD. Enhancement of barrier properties of cement mortar with graphene nanoplatelet. Cement Concr Res 2015;76:10–9. https://doi.org/10.1016/j.cemconres.2015.05.007.

[57] Du H, Gao HJ, Pang SD. Improvement in concrete resistance against water and chloride ingress by adding graphene nanoplatelet. Cement Concr Res 2016;83:114–23. https://doi.org/10.1016/j.cemconres.2016.02.005.

[58] Fediuk R, Amran M, Vatin N, Vasilev Y, Lesovik V, Ozbakkaloglu T. Acoustic properties of innovative concretes: a review. Materials 2021;14:398.

[59] Zhang Z, Provis JL, Reid A, Wang H. Mechanical, thermal insulation, thermal resistance and acoustic absorption properties of geopolymer foam concrete. Cem Concr Compos 2015;62:97–105. https://doi.org/10.1016/j.cemconcomp.2015.03.013.

[60] N. Neithalath and J. Olek JW. Acoustically Efficient Concretes Through Engineered Pore Structure. ACI Symp Publ n.d.;vol. 226. https://doi.org/10.14359/14395.

[61] Laukaitis A, Fiks B. Acoustical properties of aerated autoclaved concrete. Appl Acoust 2006;67:284–96. https://doi.org/10.1016/j.apacoust.2005.07.003.
[62] Sharma R, Varade D, Bahadur P. Mixed micelles of Triton X-100 and sodium dodecyl sulfate and their interaction with polymers. J Dispersion Sci Technol 2003; 24:53–61. https://doi.org/10.1081/DIS-120017943.
[63] El-Aila HJY. Interaction of nonionic surfactant Triton-X-100 with ionic surfactants. J Dispersion Sci Technol 2009;30:1277–80.
[64] AttarHamed F, Zoveidavianpoor M. The foaming behavior and synergistic effect in aqueous CO2 foam by in situ physisorption of alpha olefin sulfonate and Triton X-100 surfactants and their mixture. Petrol Sci Technol 2014;32:2376–86. https://doi.org/10.1080/10916466.2013.831874.
[65] Thakkar K, Bharatiya B, Ray D, Aswal VK, Bahadur P. Molecular interactions involving aqueous Triton X-100 micelles and anionic surfactants: investigations on surface activity and morphological transitions. J Mol Liq 2016;223:611–20. https://doi.org/10.1016/j.molliq.2016.08.086.
[66] LUO X, LI W, JIN X, ZENG L. Effects of porosity and pore size on sound absorption characteristic of ceramsite porous material. J Chin Ceram Soc 2011;39:158–63.
[67] Kang S, Choi JY, Choi S. Mechanism of heat transfer through porous media of inorganic intumescent coating in cone calorimeter testing. Polymers 2019;11:221.